

SANDIA REPORT

SAND2016-4733
Unlimited Release
Printed May, 2016

Element Verification and Comparison in Sierra/Solid Mechanics Problems

William Roth, Yuki Ohashi

Prepared by
Sandia National Laboratories
Albuquerque, New Mexico 87185 and Livermore, California 94550

Sandia National Laboratories is a multi-program laboratory managed and operated by Sandia Corporation, a wholly owned subsidiary of Lockheed Martin Corporation, for the U.S. Department of Energy's National Nuclear Security Administration under contract DE-AC04-94AL85000.

Approved for public release; further dissemination unlimited.

Issued by Sandia National Laboratories, operated for the United States Department of Energy by Sandia Corporation.

NOTICE: This report was prepared as an account of work sponsored by an agency of the United States Government. Neither the United States Government, nor any agency thereof, nor any of their employees, nor any of their contractors, subcontractors, or their employees, make any warranty, express or implied, or assume any legal liability or responsibility for the accuracy, completeness, or usefulness of any information, apparatus, product, or process disclosed, or represent that its use would not infringe privately owned rights. Reference herein to any specific commercial product, process, or service by trade name, trademark, manufacturer, or otherwise, does not necessarily constitute or imply its endorsement, recommendation, or favoring by the United States Government, any agency thereof, or any of their contractors or subcontractors. The views and opinions expressed herein do not necessarily state or reflect those of the United States Government, any agency thereof, or any of their contractors.

Printed in the United States of America. This report has been reproduced directly from the best available copy.

Available to DOE and DOE contractors from
U.S. Department of Energy
Office of Scientific and Technical Information
P.O. Box 62
Oak Ridge, TN 37831

Telephone: (865) 576-8401
Facsimile: (865) 576-5728
E-Mail: reports@adonis.osti.gov
Online ordering: <http://www.osti.gov/bridge>

Available to the public from
U.S. Department of Commerce
National Technical Information Service
5285 Port Royal Rd
Springfield, VA 22161

Telephone: (800) 553-6847
Facsimile: (703) 605-6900
E-Mail: orders@ntis.fedworld.gov
Online ordering: <http://www.ntis.gov/help/ordermethods.asp?loc=7-4-0#online>



Element Verification and Comparison in Sierra/Solid Mechanics Problems

William Roth, Yuki Ohashi

Abstract

The goal of this project was to study the effects of element selection on the Sierra/SM solutions to five common solid mechanics problems. A total of nine element formulations were used for each problem. The models were run multiple times with varying spatial and temporal discretization in order to ensure convergence. The first four problems have been compared to analytical solutions, and all numerical results were found to be sufficiently accurate. The penetration problem was found to have a high mesh dependence in terms of element type, mesh discretization, and meshing scheme. Also, the time to solution is shown for each problem in order to facilitate element selection when computer resources are limited.

Acknowledgments

We would like to acknowledge the support of the Sierra/SM code team for their support and responsiveness. We would like to thank Jay Foulk and Jake Ostien for contributing ideas and support of the composite tet element, and we would especially like to thank Mike Veilleux for both his involvement in code support as well as his detailed review and editing of the final document. Finally, we would like to acknowledge the funding support received from the ASC V&V program.

Contents

1	Introduction	13
2	Propped Cantilever	15
2.1	Model Description	15
2.2	Results	16
2.2.1	Hex8 Results	16
2.2.2	Tet4 and Tet10 Results	17
2.3	Element Comparison	18
3	Non-linear Material Model	21
3.1	Model Description	21
3.2	Results	22
3.2.1	Hex8 Mean Quadrature Results	23
3.2.2	Hex8 Selective Deviatoric Results	24
3.2.3	Hex8 Q1P0 Results	26
3.2.4	Hex8 Fully Integrated Results	26
3.2.5	Tet4 Mean Quadrature Results	27
3.2.6	Tet4 Nodal Based Results	29
3.2.7	Tet10 Mean Quadrature Results	31
3.2.8	Tet10 Fully Integrated Results	32
3.2.9	Tet10 Composite Results	34
3.3	Element Comparison	35

4	Impact Model	39
4.1	Model Description	39
4.2	Results	40
5	Friction Model	43
5.1	Model Description	43
5.2	Results	45
6	Penetration Model	49
6.1	Model Description	49
6.2	Results	49
6.2.1	Tetrahedral Discretization 1	50
6.2.2	Tetrahedral Discretization 2	50
6.2.3	Tetrahedral Discretization 3	56
6.2.4	Hexahedral Mesh 1	56
6.2.5	Mesh Dependence	59
6.2.6	Hexahedral Mesh 2 Discretization 1	60
6.2.7	Hexahedral Mesh 2 Discretization 2	60
6.3	Element Comparison	63
7	Conclusions	69
	References	70

List of Figures

2.1	Propped cantilever, meshing scheme.	16
2.2	Propped cantilever model, hex timing studies.	18
2.3	Propped cantilever model, tet timing studies.	19
3.1	Nonlinear material model, meshing scheme.	22
3.2	Hex8 mean quadrature, stress-strain diagram for nonlinear material model problem	23
3.3	Hex8 selective deviatoric, stress-strain diagram for nonlinear material model problem	24
3.4	Hex8 Q1P0, stress-strain diagram for nonlinear material model problem.	26
3.5	Hex8 fully integrated element, stress-strain diagram for the nonlinear material model problem.	27
3.6	Stress-strain diagram for tet4, mean quadrature element for the nonlinear material model problem	29
3.7	Stress-strain diagram for tet4, nodal based element for the nonlinear material model problem	31
3.8	Stress-strain diagram for tet10, mean quadrature element for the nonlinear material model problem.	32
3.9	Stress-strain diagram for tet10, fully integrated element for nonlinear material model problem.	34
3.10	Stress-strain diagram for tet10, composite element for the nonlinear material model problem.	35
3.11	Nonlinear material model, hex8 element comparison of wall time.	37
3.12	Nonlinear material model, tetrahedral element comparison of wall time.	38
4.1	Impact model setup	39
4.2	Impact model meshing scheme.	40

4.3	Impact model, hexahedral element comparison of wall time.....	41
4.4	Impact model, tetrahedral element comparison of wall time.	42
5.1	Friction model setup.....	43
5.2	Friction model meshing scheme.	44
5.3	Friction model, element comparison of numerical error	45
5.4	Friction model, hexahedral element comparison of wall time.	46
5.5	Friction model, tetrahedral element comparison of wall time	47
6.1	Penetration model, setup.	50
6.2	Penetration model, tet4 mean quadrature, discretization 1.	51
6.3	Penetration model, tet4 nodal based, discretization 1.....	51
6.4	Penetration model, tet10 mean quadrature, discretization 1.	52
6.5	Penetration model, tet10 fully integrated, discretization 1.....	52
6.6	Penetration model, tet10 composite, discretization 1.	53
6.7	Penetration model, tet4 mean quadrature, discretization 2.	53
6.8	Penetration model, tet4 nodal based, discretization 2.....	54
6.9	Penetration model, tet10, mean quadrature, discretization 2.	54
6.10	Penetration model, tet10, fully integrated, discretization 2.	55
6.11	Penetration model, tet10, composite, discretization 2.....	55
6.12	Penetration model, tet4, mean quadrature, discretization 3.....	56
6.13	Penetration model, tet4, nodal based, discretization 3.	57
6.14	Penetration model, hex8, mean quadrature, mesh 1, discretization 1.	57
6.15	Penetration model, hex8, selective deviatoric, mesh 1, discretization 1.	58
6.16	Penetration model, hex8, Q1P0, mesh 1, discretization 1.....	58
6.17	Penetration model, hex8, fully integrated, mesh 1, discretization 1.....	59
6.18	Penetration model, comparison of hex meshing schemes	60

6.19	Penetration model, mean quadrature hex8 mesh 1, increasing discretization . . .	61
6.20	Penetration model, mean quadrature hex8 mesh 2, discretization 1.	61
6.21	Penetration model, selective deviatoric hex8 mesh 2, discretization 1.	62
6.22	Penetration model, Q1P0 hex8 mesh 2, discretization 1.	62
6.23	Penetration model, fully integrated hex8 mesh 2, discretization 1.	63
6.24	Penetration model, mean quadrature hex8 mesh 2, discretization 2.	64
6.25	Penetration model, selective deviatoric hex8 mesh 2, discretization 2.	64
6.26	Penetration model, Q1P0 hex8 mesh 2, discretization 2.	65
6.27	Penetration model, fully integrated hex8 mesh 2, discretization 2.	65
6.28	Penetration model, comparison between elements.	66
6.29	Penetration model, hex element comparison of wall time.	67
6.30	Penetration model, tet element comparison of wall time.	68

List of Tables

1.1	Element types	13
2.1	Percent error of results from propped cantilever hexahedral models.	17
2.2	Percent error of results from propped cantilever tetrahedral models.	17
3.1	Hex8 mean quadrature, nonlinear material model results with spatial discretization.	23
3.2	Hex8 mean quadrature, nonlinear material model results with temporal discretization.	24
3.3	Hex8 selective deviatoric, nonlinear material model results with spatial discretization.	25
3.4	Hex8 selective deviatoric, nonlinear material model results with temporal discretization.	25
3.5	Hex8 Q1P0, nonlinear material model results with spatial discretization.	26
3.6	Hex8 Q1P0, nonlinear material model results with temporal discretization.	27
3.7	Hex8 fully integrated, nonlinear material model results with spatial discretization.	28
3.8	Hex8 fully integrated, nonlinear material model results with temporal discretization.	28
3.9	Tet4 mean quadrature, nonlinear material model results with spatial discretization.	29
3.10	Tet4 mean quadrature, nonlinear material model results with temporal discretization.	30
3.11	Tet4 nodal based, nonlinear material model results with spatial discretization.	30
3.12	Tet4 nodal based, nonlinear material model results with temporal discretization.	30
3.13	Tet10 mean quadrature, nonlinear material model results with spatial discretization.	31

3.14 Tet10 mean quadrature, nonlinear material model results with temporal discretization.	32
3.15 Tet10 fully integrated, nonlinear material model results with spatial discretization.	33
3.16 Tet10 fully integrated, nonlinear material model results with temporal discretization.	33
3.17 Tet10 composite, nonlinear material model results with spatial discretization.	34
3.18 Tet10 composite, nonlinear material model results with temporal discretization.	35
3.19 Nonlinear material model, solution wall time (seconds) for hex8 elements with spatial discretization.	36
3.20 Nonlinear material model, solution wall time (seconds) for tetrahedral elements with spatial discretization.	36

Chapter 1

Introduction

This project is focused on verifying a group of elements for five solid mechanics problems using the Sierra/SM framework. The nine element formulations used are shown in Table 1.1. Five different problems were chosen: propped cantilever beam under point loading, nonlinear material model, impact model, friction model, and a penetration model. Each model was designed to test a common feature within Sierra, such as nonlinear material model, contact, friction or element death. The models were run with all nine element formulations and included increasing spatial and temporal discretization in order to verify convergence and compare the accuracy of the numerical solution between elements. The elements were also compared with respect to simulation efficiency in order to make appropriate element selections. The following sections will discuss in detail each of the five models, the numerical solutions, and an element comparison. All analyses, unless otherwise noted, were run in Sierra v4.34 on a local Linux workstation or on the High Performance Computing Linux clusters redsky or uno. For all analyses, the deviatoric parameter for the hex8 selective deviatoric element formulation was set to 0.5.

Table 1.1. Element types

Element Shape	Formulation
8 noded hexahedral	Mean quadrature Selective deviatoric Q1P0 Fully integrated
4 noded tetrahedral	Mean quadrature Nodal Based
10 noded tetrahedral	Mean quadrature Fully integrated Composite

Chapter 2

Propped Cantilever

2.1 Model Description

The propped cantilever model was subjected to a quasi-static concentrated load at a specified distance from the propped end. The beam had a 1 inch square cross section and was 30 inches long. A 100 lb load was applied as a traction on a cross section of the beam at a distance of 9 inches from the propped end. This loading method allowed for a given value of the point load while avoiding issues at the load location sometimes seen with point loading of finite element models. An implicit solution method was applied.

The mesh size was controlled by the number of elements along the edges of the beam. The mesh densities used in the simulations were 2, 8 and 16 elements through the cross section, shown in Figure 2.1. An attempt was made to standardize the number of processors used in the analyses so that a direct comparison of run times could be made, without regard to possible input/output or processor communication considerations. The nodal based tet and the composite tet, however, required some adjusting of target and acceptable residual values and number of processors in order to run, so the time to completion comparisons between models may not be direct.

The mechanical properties were as follows: Young's modulus of 10.e6 psi, and Poisson's ratio of 0.3. The elastic material model in Sierra/SM, a hypo-elastic model capturing linear elastic behavior, was used.

The displacement in the y-direction under the point of loading was used as the accuracy metric for this analysis. Assuming small deformations and using Euler-Bernoulli beam theory, the displacement under the load point can be calculated from the following equation:

$$\begin{aligned} dy &= \frac{Pa^2b^3}{12EI^3}(3l + a), \text{ where} \\ P &= \text{applied load,} \\ a &= \text{distance from load to propped end,} \\ b &= \text{distance from load to cantilever end,} \\ l &= \text{beam length,} \\ E &= \text{modulus of elasticity, and} \\ I &= \text{moment of inertia.} \end{aligned} \tag{2.1}$$

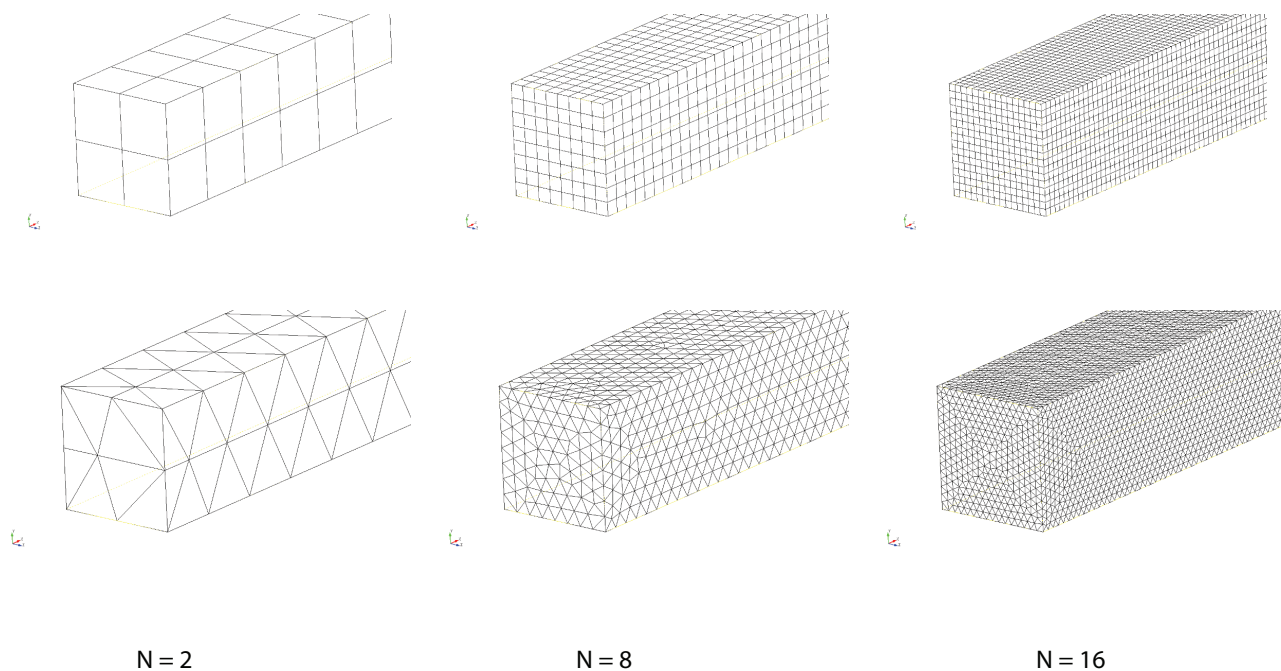


Figure 2.1. Propped cantilever, meshing scheme.

2.2 Results

All of the elements successfully completed the elastic bending problem. The error remained relatively small for all cases, except for meshes with two elements through the thickness, many of which had errors on the order of 10%. Of those two element meshes, the Q1P0 hex8 as well as the fully integrated tet10 and the composite tet10 had errors on the order of 1%. The errors dropped precipitously with an increase in mesh density, and with all nine element types used, the error was less than 1% for models with the highest mesh density.

2.2.1 Hex8 Results

All formulations of the 8 noded hexahedral element successfully ran for all discretization cases, and the numerical error was small for all except the most coarse mesh. The errors on the results for the hex8 propped cantilever runs can be found in Table 2.1.

Table 2.1. Percent error of results from propped cantilever hexahedral models.

Element Type	N = 2	N = 8	N = 16
Mean Quadrature	18.8	1.5	0.7
Selective Deviatoric	13.1	1.2	0.7
Q1P0	-1.3	0.3	0.4
Fully Integrated	-11.7	-0.4	0.3

Table 2.2. Percent error of results from propped cantilever tetrahedral models.

Element Type	N = 2	N = 8	N = 16
Mean Quadrature Tet4	-24.4	-2.4	-0.2
Nodal Based Tet4	14.8	1.0	0.6
Mean Quadrature Tet10	-8.3	-0.5	0.2
Fully Integrated Tet10	0.4	0.5	0.5
Composite Tet10	-0.4	0.4	0.5

2.2.2 Tet4 and Tet10 Results

Both formulations of the 4 noded tetrahedral element successfully ran for all discretization cases, and the numerical error was small for all except the most coarse mesh. The nodal based tet required some adjusting of the target and acceptable residuals in order to converge. A large acceptable relative residual was included such that the first few time steps would converge, after which the relative residuals decreased to reasonable levels.

The 10 noded tetrahedral element successfully ran for all discretization cases, and the numerical error was small across the board. The most refined mesh using composite tets required a particular number of processors in order to converge; the issue was noted in a user support ticket for Sierra/SM. The small errors for even the most coarse mesh for the fully integrated and composite tet10 models indicate that these two element types do not require a highly refined mesh in order to achieve mesh convergent results as the tet4 elements or the standard tet10 typically require. Errors for the models using tetrahedral elements can be found in Table 2.2.

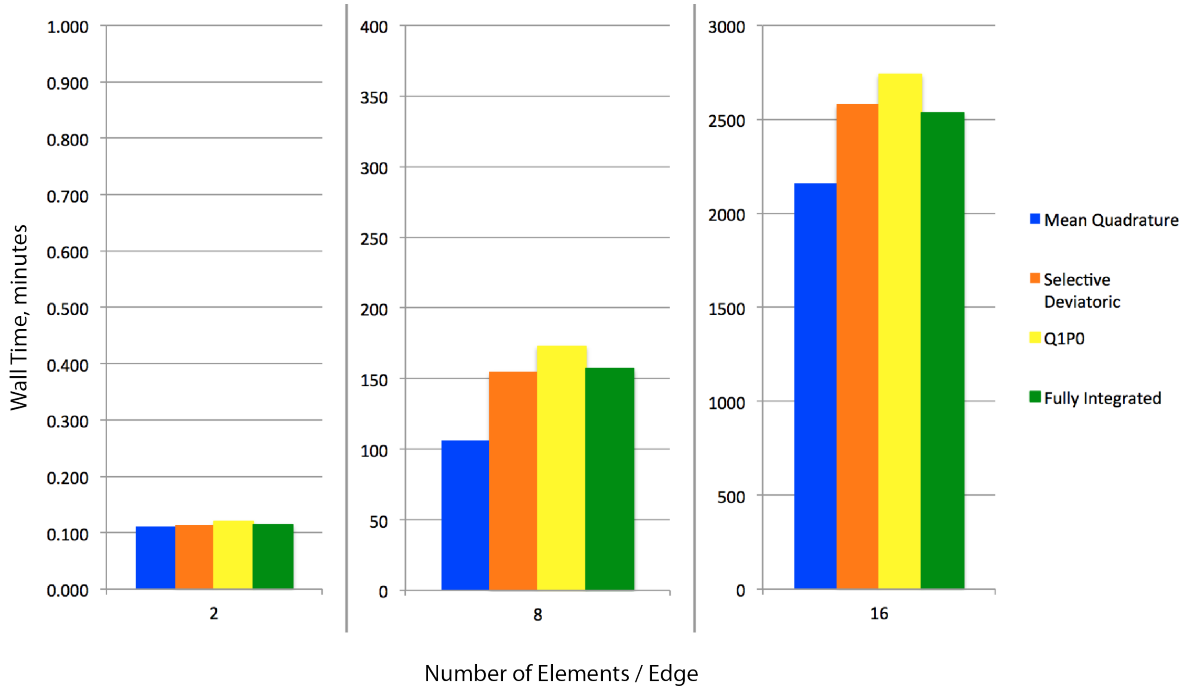


Figure 2.2. Propped cantilever model, hex timing studies.

2.3 Element Comparison

All runs for the propped cantilever model were performed in Adagio v4.36.1 on the computing cluster redsky. As noted previously, an effort was made to standardize the runs such that a direct comparison could be made with respect to run times; however, the larger tetrahedral meshes provided some challenges in that regard. All except the medium and refined tet4 and tet10 models were analyzed using 4 processors. The medium and refined tetrahedral models were analyzed using 128 processors. The total wall time plotted in Figures 2.2 and 2.3 includes time used for all processors, i.e. time to run multiplied by the number of processors used.

For all mesh refinements, the mean quadrature hex had the shortest run time, and the Q1P0 hex element had the longest run time. The selective deviatoric and fully integrated hex elements had relatively similar run times and were in between the two extremes.

The standard tet4 element was the fastest of the tet elements for each mesh refinement. Of the tet10 element formulations, different mesh refinements yielded different results; however, the fully integrated tet10 was the most consistently fast across different mesh refinements. For the most refined mesh, the standard tet10 required significantly more iterations per time step, in an attempt to reduce the relative residual, than the fully integrated tet10. A slightly more lenient acceptable relative residual may allow for faster convergence, but it is unclear

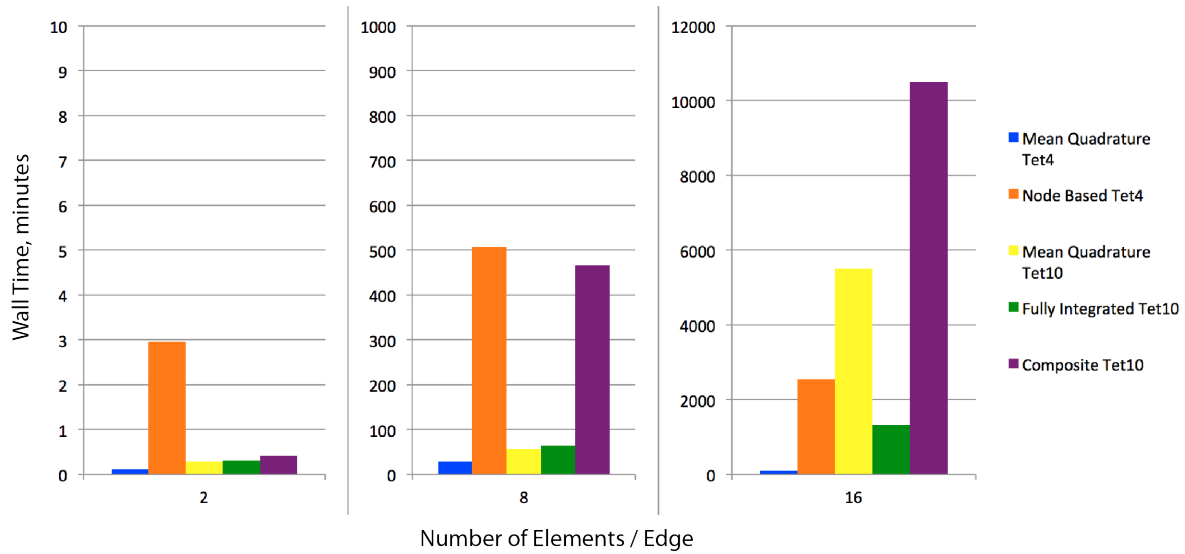


Figure 2.3. Propped cantilever model, tet timing studies.

why the standard tet10 element performed so poorly compared with the fully integrated tet10 for the same relative residual. Regardless, the small difference in timing for other mesh refinements as well as the small errors, even with the most coarse mesh, would indicate that using the fully integrated tet10 over the standard tet10 should provide adequate results in a comparable length of time. Composite tet timing issues are being investigated by the Sierra/SM code team. The composite tet in this example required a smaller time step and looser convergence criteria in order to converge; this may contribute to the unexpected longer run times seen in this problem.

Chapter 3

Non-linear Material Model

3.1 Model Description

In this problem set a one inch cube is subjected to a uniaxial tensile load along the Y axis in order to test the nonlinear material model functionality of each element. The negative Y surface of the cube was fixed in the Y direction, while a fixed velocity of 20 inches per second was applied to the positive Y surface in the positive Y direction. The simulation was run to a termination time of one millisecond. Explicit transient dynamics was applied.

The mesh size was controlled by the number of elements along the edges of the cube. The mesh densities used in the simulations were 2, 4, 8 and 16 elements along the edges. Figure 3.1 shows the mesh refinements for the hex and tet models of the non-linear material model test.

In addition to considering the spatial discretization of the problem, the temporal discretization was also considered for convergence. The temporal discretization used the N=8 discretization of the mesh, while the time step was varied. The first run used the automatic time step calculation, the the second and third runs used one half and one fourth of this time step, respectively.

The material properties used in Sierra/SM's elastic-plastic material model were as follows: density of $7.4e-4$ slinches per cubic inch, Young's modulus of 29 Msi, Poisson's ratio of 0.3, yield stress of 30 ksi, hardening modulus of 10 Msi, and a beta parameter of 1.0.

In order to verify the accuracy of the solution, the Young's modulus and hardening modulus are calculated from the output variables and compared to the input values. The normal log strain and the normal Cauchy stress in the Y direction at the center of the cube were used to generate a stress-strain diagram. Then, the Young's modulus was determined by calculating the slope in the elastic regime and the tangent modulus from the plastic regime. Then, the hardening modulus is calculated from these two metrics through equation 3.1. The elastic modulus was calculated by picking a point just below the yield stress and a point at the start of loading and calculating the slope; if there were errors in the solution around the transition between elastic and plastic regimes, the calculated results may be affected.

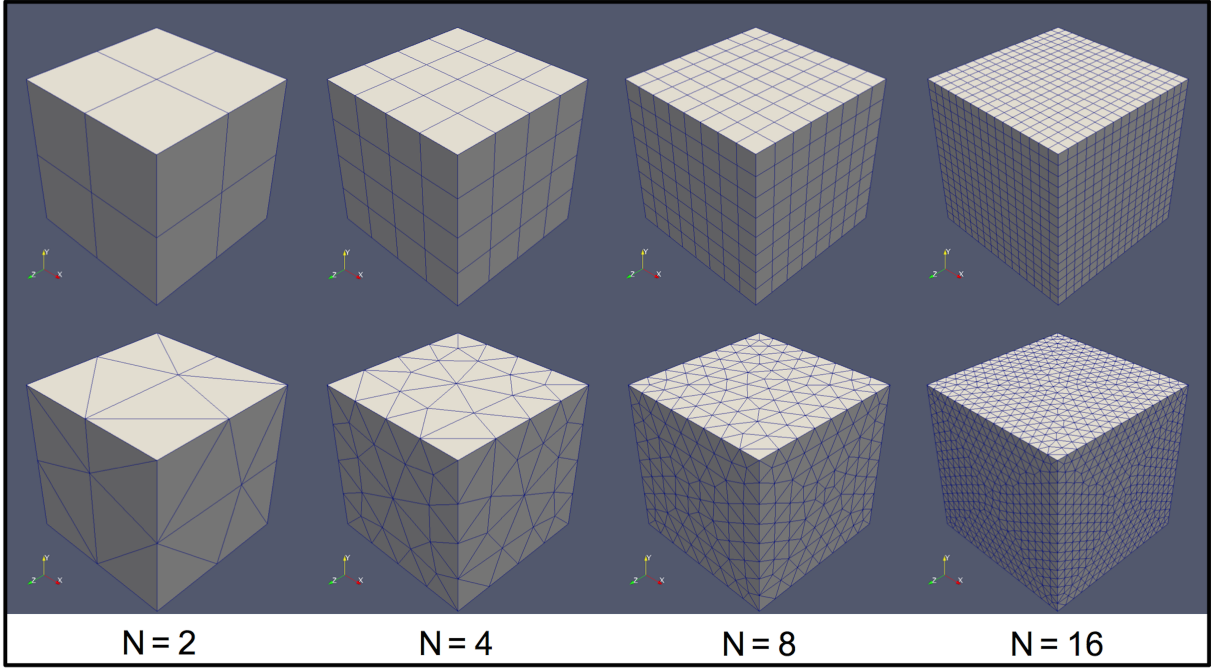


Figure 3.1. Nonlinear material model, meshing scheme.

$$H = \frac{E^*E^T}{E - E^T} \quad (3.1)$$

The numerical Young's modulus and hardening modulus are then compared to the values which were used in the input deck.

3.2 Results

All of the elements successfully implemented the nonlinear material model. The error remained adequately small for all cases, except for a few of the most coarse meshes that had errors of a few percent. Most of the error occurs in near the yield stress during the transition from elastic to plastic regime. Beyond the first increase in spatial discretization, the magnitude of the error does not necessarily decrease with an increase in either spatial or temporal discretization. The stress and strain variables were output through paraview by specifies a spatial coordinate; therefore, some error could have been introduced if the spatial coordinate was located between elements and the strain and stress variables were pulled from different elements. For elements with multiple integration points, the results from the first integration point are presented. The following sections will discuss the detailed results from each element.

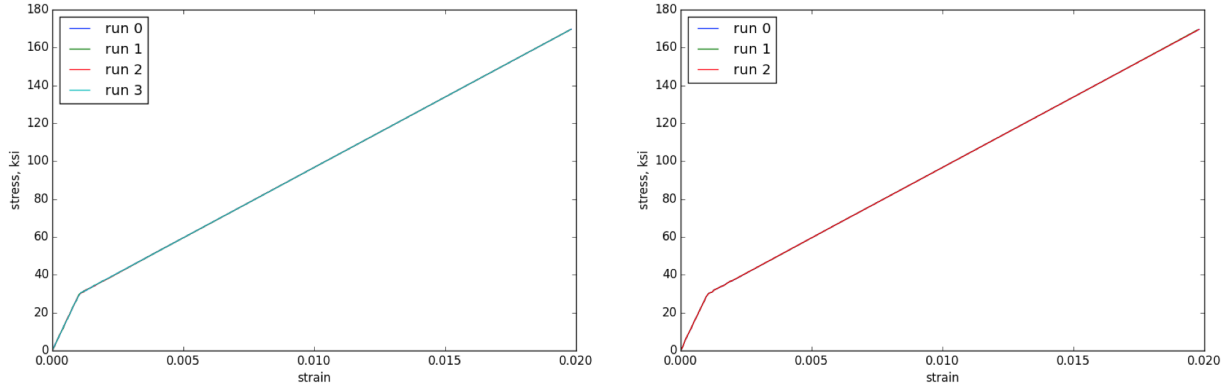


Figure 3.2. Hex8 mean quadrature, stress-strain diagram for non-linear material model (a) spatial discretization with $N=2, 4, 8,$ and $16,$ and (b) temporal discretization of $N=8$ mesh.

3.2.1 Hex8 Mean Quadrature Results

The 8 noded hexahedral element with a mean quadrature formulation successfully ran for all discretization cases, and the numerical error was small across the board. Figure 3.2 shows the numerical stress-strain diagram for this simulation. On the left side of the illustration is the spatial discretization case, while the right side has the temporal discretization results. Table 3.1 shows the elastic modulus and plastic modulus results for the spatial discretization runs, along with the error. Table 3.2 has the results for the temporal discretization runs.

Table 3.1. Hex8 mean quadrature, nonlinear material model results with spatial discretization.

Relative Element Length	Numerical Elastic Modulus, Msi	Numerical Error %,	Numerical Plastic Modulus, Msi	Numerical Error %,
1/2	28.92	0.27	9.99	0.12
1/4	29.21	0.73	9.97	0.35
1/8	29.14	0.48	10.02	0.23
1/16	29.04	0.12	10.01	0.09

Table 3.2. Hex8 mean quadrature, nonlinear material model results with temporal discretization.

Relative Time Step	Numerical Elastic Modulus, Msi	Numerical Error %,	Numerical Plastic Modulus, Msi	Numerical Error %,
1	29.14	0.48	10.02	0.23
1/2	29.17	0.57	10.04	0.41
1/4	29.16	0.57	10.02	0.21

3.2.2 Hex8 Selective Deviatoric Results

All cases of the 8 noded hexahedral element with selective deviatoric formulation ran successfully. The first spatial discretization had an error of just over one percent for the elastic modulus, but this error decreased with a denser mesh. The stress-strain diagrams are shown in Figure 3.3, where the left plot is the spatial discretization, and the right plot is the temporal discretization. The results and error for the spatial discretization runs are listed in Table 3.3, while the temporal discretization runs are listed in Table 3.4.

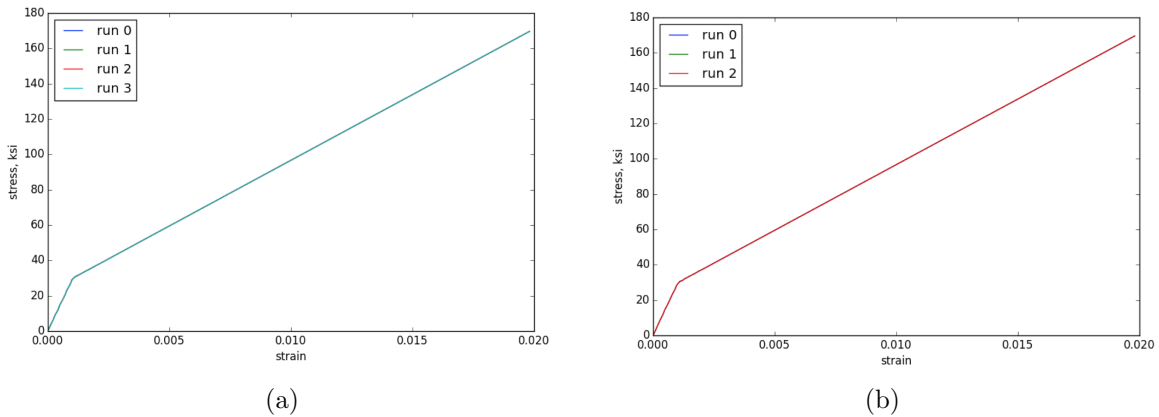


Figure 3.3. Hex8 selective deviatoric, stress-strain diagram (a) spatial discretization with $N=2, 4, 8,$ and $16,$ and (b) temporal discretization with $N=8.$

Table 3.3. Hex8 selective deviatoric, nonlinear material model results with spatial discretization.

Relative Element Length	Numerical Elastic Modulus, Msi	Numerical Error %,	Numerical Plastic Modulus, Msi	Numerical Error %,
1/2	29.36	1.25	9.95	0.48
1/4	28.95	0.17	9.99	0.11
1/8	29.11	0.38	10.01	0.07
1/16	29.04	0.12	10.00	0.04

Table 3.4. Hex8 selective deviatoric, nonlinear material model results with temporal discretization.

Relative Time Step	Numerical Elastic Modulus, Msi	Numerical Error %,	Numerical Plastic Modulus, Msi	Numerical Error %,
1	29.11	0.38	10.01	0.07
1/2	29.08	0.28	10.02	0.17
1/4	29.08	0.28	10.02	0.16

Table 3.5. Hex8 Q1P0, nonlinear material model results with spatial discretization.

Relative Element Length	Numerical Elastic Modulus, Msi	Numerical Error %,	Numerical Plastic Modulus, Msi	Numerical Error %,
1/2	29.11	0.40	9.91	0.86
1/4	27.69	4.52	10.19	1.87
1/8	29.00	0.003	10.07	0.73
1/16	28.90	0.34	10.01	0.07

3.2.3 Hex8 Q1P0 Results

The Q1P0 formulation was successful, except for the second spatial discretization, where the numerical error for the elastic modulus exceeded four percent, and the numerical error for the plastic modulus exceeded one percent. The stress-strain diagrams are shown in Figure 3.4, and the numerical results and errors are listed in Table 3.5 and Table 3.6 for the spatial discretization runs and temporal discretization runs, respectively.

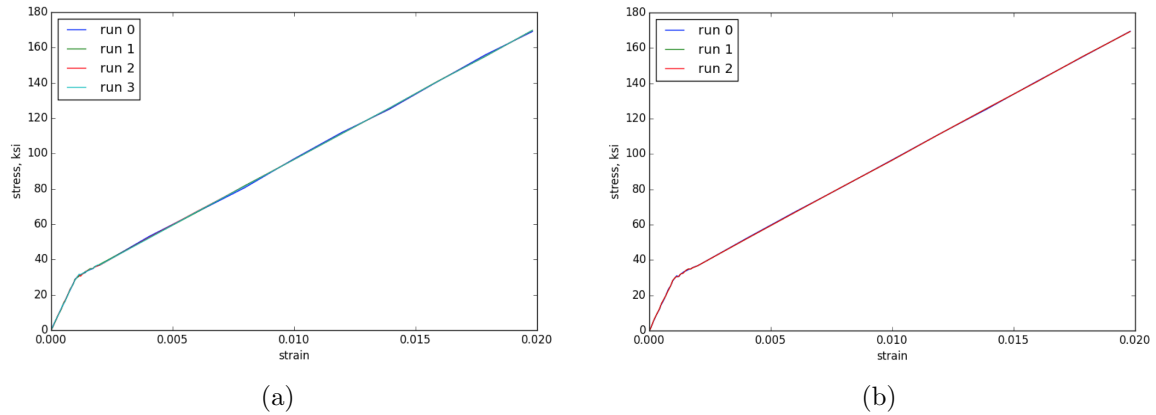


Figure 3.4. Hex8 Q1P0, stress-strain diagram (a) spatial discretization with $N=2, 4, 8,$ and $16,$ and (b) temporal discretization with $N=8.$

3.2.4 Hex8 Fully Integrated Results

The fully integrated formulation had some issues with the first and third spatial discretization runs. On the first run, the elastic modulus error was over three percent and the plastic

Table 3.6. Hex8 Q1P0, nonlinear material model results with temporal discretization.

Relative Time Step	Numerical Elastic Modulus, Msi	Numerical Error %,	Numerical Plastic Modulus, Msi	Numerical Error %,
1	29.00	0.003	10.07	0.73
1/2	29.29	1.01	10.02	0.16
1/4	29.29	1.01	10.02	0.17

modulus error was over four percent. Also, the slope in the plastic regime should be linear; however, the stress seems to oscillate around the expected values, as seen in Figure 3.5. The third spatial discretization run has an elastic modulus error of almost six percent. Most of the errors are attributed to discrepancies around the transition from elastic to plastic regime. None of the element cases have completely smooth transitions through the yield stress. Results and errors for the spatial and temporal discretizations of the nonlinear material model problem are listed in Table 3.7 and Table 3.8.

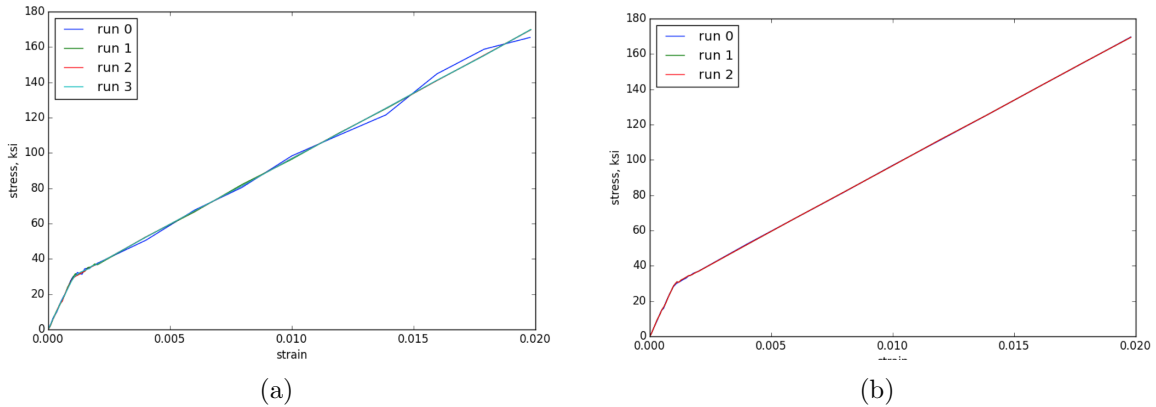


Figure 3.5. Hex8 fully integrated element, stress-strain diagram (a) spatial discretization with $N=2, 4, 8,$ and $16,$ and (b) temporal discretization with $N=8.$

3.2.5 Tet4 Mean Quadrature Results

The four noded tetrahedral with a mean quadrature formulation successfully ran for all cases. The first spatial discretization run had almost five percent error for the elastic modulus; however, this error decreased with increasing spatial discretization. The stress-strain

Table 3.7. Hex8 fully integrated, nonlinear material model results with spatial discretization.

Relative Element Length	Numerical Elastic Modulus, Msi	Numerical Error %,	Numerical Plastic Modulus, Msi	Numerical Error %,
1/2	29.91	3.14	9.54	4.61
1/4	28.96	0.12	10.09	0.89
1/8	27.29	5.91	10.28	2.83
1/16	28.49	1.77	10.09	0.92

Table 3.8. Hex8 fully integrated, nonlinear material model results with temporal discretization.

Relative Time Step	Numerical Elastic Modulus, Msi	Numerical Error %,	Numerical Plastic Modulus, Msi	Numerical Error %,
1	27.29	5.91	10.28	2.83
1/2	29.08	0.28	10.04	0.40
1/4	29.10	0.34	10.04	0.38

Table 3.9. Tet4 mean quadrature, nonlinear material model results with spatial discretization.

Relative Element Length	Numerical Elastic Modulus, Msi	Numerical Error %,	Numerical Plastic Modulus, Msi	Numerical Error %,
1/2	27.64	4.70	10.18	1.75
1/4	28.51	1.68	10.09	0.88
1/8	29.00	0.005	10.00	0.01
1/16	29.07	0.24	10.01	0.05

diagrams are shown in Figure 3.6, where the spatial discretization is on the left side and the temporal discretization is on the right. The numerical results and errors for the tet4 models are listed in Table 3.9 and Table 3.10.

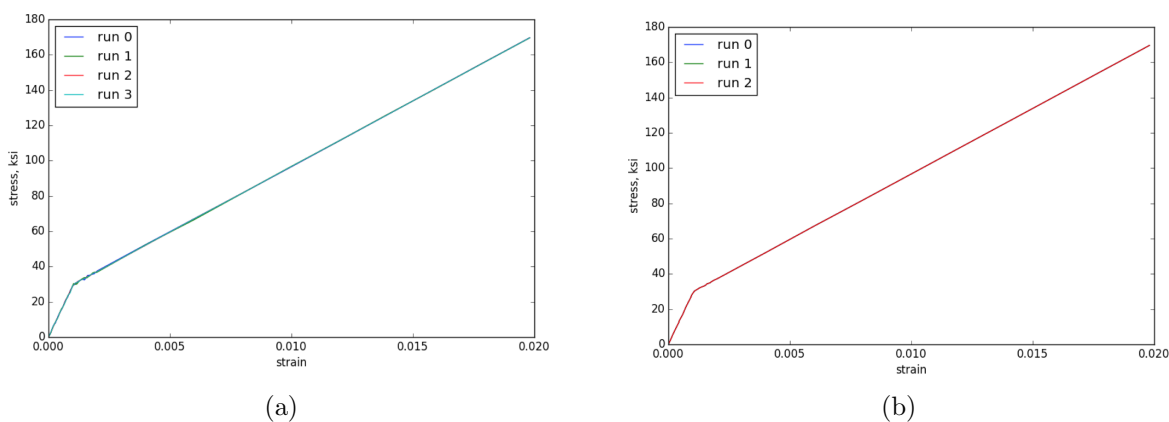


Figure 3.6. Stress-strain diagram for tet4, mean quadrature element (a) spatial discretization with $N=2, 4, 8,$ and $16,$ and (b) temporal discretization.

3.2.6 Tet4 Nodal Based Results

The nodal based formulation of the four noded tetrahedral provided slightly better results than the mean quadrature formulation. The maximum elastic modulus error decreased from almost five percent for the standard tet4 element to just over two percent for the nodal based tet. The stress-strain diagrams are shown in Figure 3.7, and the numerical results and errors are listed in Table 3.11 and Table 3.12.

Table 3.10. Tet4 mean quadrature, nonlinear material model results with temporal discretization.

Relative Time Step	Numerical Elastic Modulus, Msi	Numerical Error %,	Numerical Plastic Modulus, Msi	Numerical Error %,
1	29.00	0.005	10.00	0.01
1/2	29.04	0.14	9.99	0.08
1/4	29.04	0.14	9.99	0.08

Table 3.11. Tet4 nodal based, nonlinear material model results with spatial discretization.

Relative Element Length	Numerical Elastic Modulus, Msi	Numerical Error %,	Numerical Plastic Modulus, Msi	Numerical Error %,
1/2	29.69	2.38	9.94	0.64
1/4	28.90	0.36	10.07	0.67
1/8	29.15	0.51	9.98	0.22
1/16	29.33	1.14	10.00	0.03

Table 3.12. Tet4 nodal based, nonlinear material model results with temporal discretization.

Relative Time Step	Numerical Elastic Modulus, Msi	Numerical Error %,	Numerical Plastic Modulus, Msi	Numerical Error %,
1	29.15	0.51	9.98	0.22
1/2	29.17	0.58	9.97	0.26
1/4	29.17	0.58	9.97	0.26

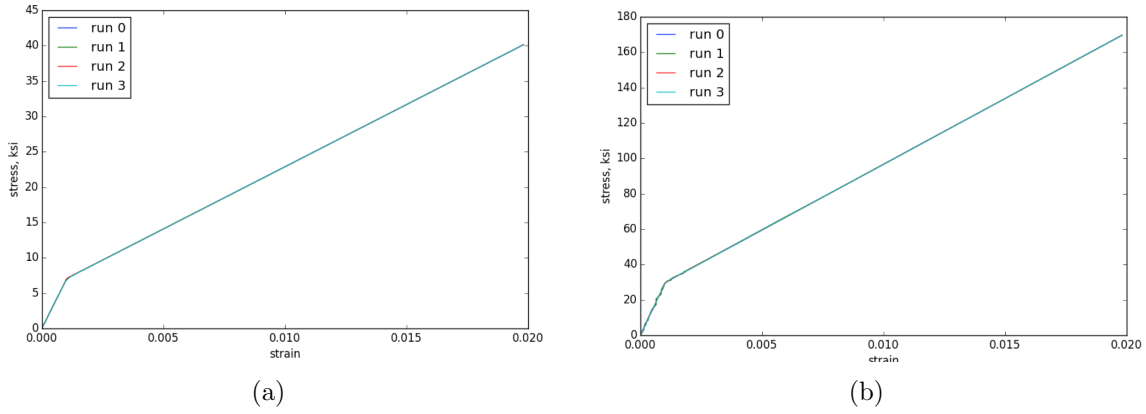


Figure 3.7. Stress-strain diagram for tet4, nodal based element (a) spatial discretization with $N=2, 4, 8,$ and $16,$ and (b) temporal discretization with $N=8.$

Table 3.13. Tet10 mean quadrature, nonlinear material model results with spatial discretization.

Relative Element Length	Numerical Elastic Modulus, Msi	Numerical Error %,	Numerical Plastic Modulus, Msi	Numerical Error %,
1/2	29.15	0.53	9.90	0.95
1/4	29.21	0.72	10.01	0.12
1/8	28.91	0.31	10.02	0.28
1/16	28.99	0.008	10.03	0.30

3.2.7 Tet10 Mean Quadrature Results

The ten noded tetrahedral with a mean quadrature formulation successfully ran for all of the discretization runs. The numerical error remained low for both the spatial and the temporal changes in discretization. The error did not decrease with increasing discretization, instead it was random. The stress-strain diagram is shown in Figure 3.8. The left side of the figure is the spatial discretization, and the right side of the figure is the temporal discretization. The results are also listed in Table 3.13, spatial discretization, and Table 3.14, temporal discretization.

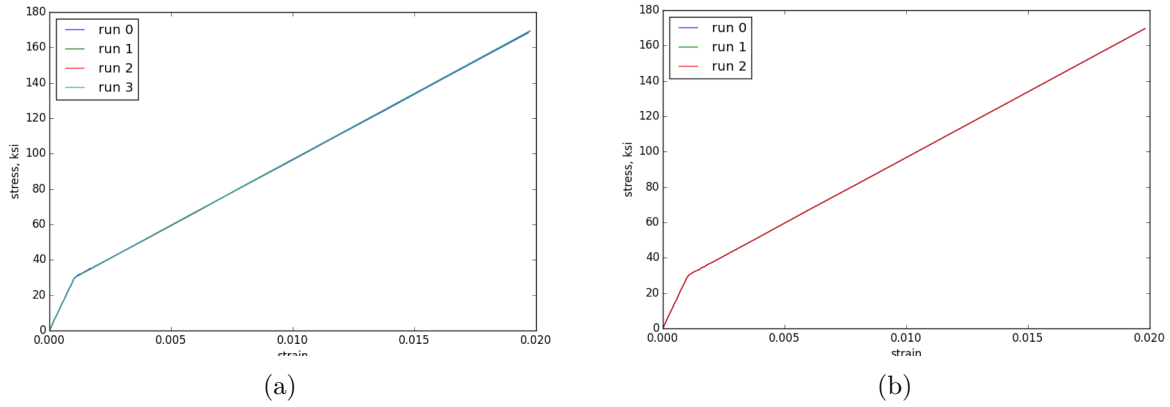


Figure 3.8. Stress-strain diagram for tet10, mean quadrature element (a) spatial discretization with $N=2, 4, 8,$ and $16,$ and (b) temporal discretization with $N=8.$

Table 3.14. Tet10 mean quadrature, nonlinear material model results with temporal discretization.

Relative Time Step	Numerical Elastic Modulus, Msi	Numerical Error %,	Numerical Plastic Modulus, Msi	Numerical Error %,
1	29.00	0.005	10.00	0.01
1/2	29.04	0.14	9.99	0.08
1/4	29.04	0.14	9.99	0.08

3.2.8 Tet10 Fully Integrated Results

The fully integrated formulation of the ten noded tetrahedral had an issue with the automatic time step calculation. If the default parameters were used for the explicit time step calculation, then excess error should build up during the run. If the simulation completed without a critical error, then the results contained significant errors. In order to overcome this issue, the initial time step was forced to be very small, then allowed to slowly increase to a reasonable value. This caused the simulation to take longer to run than expected. For the temporal discretization cases, the first run was completed with the default time step settings; therefore the results are meaningless. After the first run, the time step was set to one half and one fourth the default values, which resulted in successful simulations. The stress-strain diagrams are shown in Figure 3.9, and the numerical results and errors are listed in Table 3.15 and Table 3.16.

Table 3.15. Tet10 fully integrated, nonlinear material model results with spatial discretization.

Relative Element Length	Numerical Elastic Modulus, Msi	Numerical Error %,	Numerical Plastic Modulus, Msi	Numerical Error %,
1/2	28.44	1.95	10.11	1.06
1/4	28.75	0.86	10.07	0.65
1/8	29.34	1.17	9.95	0.50
1/16	29.14	0.51	9.99	0.12

Table 3.16. Tet10 fully integrated, nonlinear material model results with temporal discretization.

Relative Time Step	Numerical Elastic Modulus, Msi	Numerical Error %,	Numerical Plastic Modulus, Msi	Numerical Error %,
1	N/A	N/A	N/A	N/A
1/2	29.39	1.34	9.95	0.52
1/4	29.41	1.42	9.95	0.55

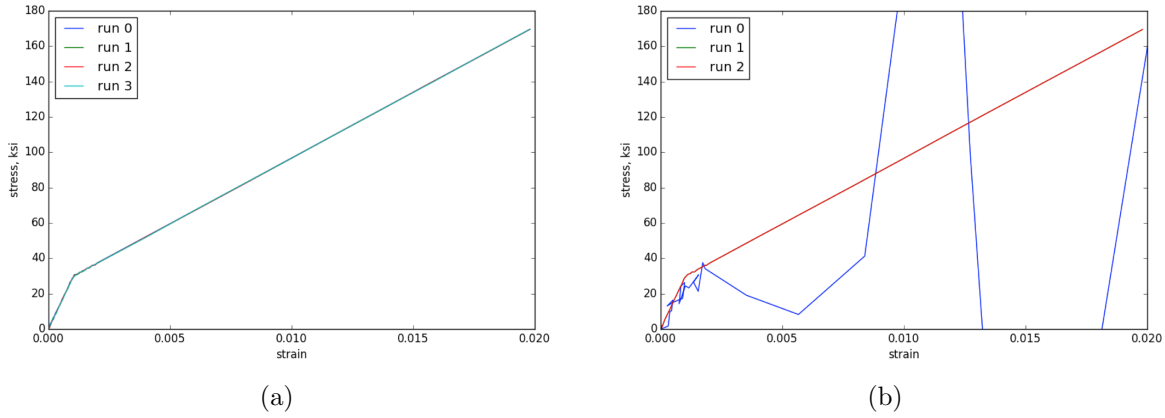


Figure 3.9. Stress-strain diagram for tet10, fully integrated element (a) spatial discretization with $N=2, 4, 8,$ and $16,$ and (b) temporal discretization with $N=8.$ Run 0 of the temporal discretization employed the automatic explicit time step and allowed excess errors to build in the solution.

3.2.9 Tet10 Composite Results

The composite tet10 simulation had some large errors for the first and second spatial discretization runs. The most coarse mesh had an elastic modulus error of about one and a half percent, while the second mesh discretization run had an elastic modulus error of over five percent. As before, these error seem to come to occur during the transition from the elastic to the plastic regime and may be due to the method of sampling the results. The stress-strain diagram is shown in Figure 3.10, and the numerical results and errors are listed in Table 3.17 and Table 3.18 .

Table 3.17. Tet10 composite, nonlinear material model results with spatial discretization.

Relative Element Length	Numerical Elastic Modulus, Msi	Numerical Error %,	Numerical Plastic Modulus, Msi	Numerical Error %,
1/2	29.42	1.44	9.92	0.77
1/4	27.45	5.33	10.18	1.81
1/8	28.91	0.30	10.00	0.01
1/16	29.10	0.33	9.99	0.05

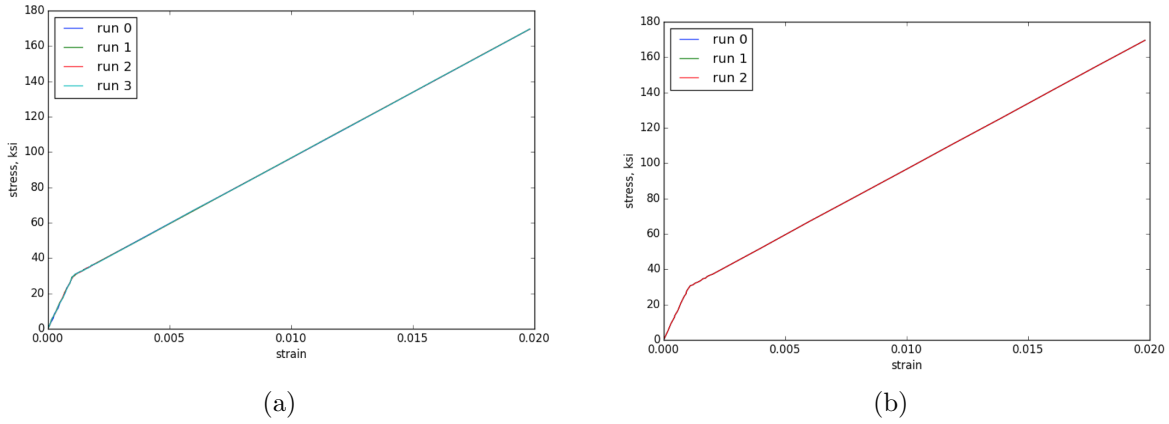


Figure 3.10. Stress-strain diagram for tet10, composite element (a) spatial discretization with $N=2, 4, 8,$ and $16,$ and (b) temporal discretization with $N=8.$

Table 3.18. Tet10 composite, nonlinear material model results with temporal discretization.

Relative Time Step	Numerical Elastic Modulus, Msi	Numerical Error %,	Numerical Plastic Modulus, Msi	Numerical Error %,
1	29.18	0.61	9.99	0.12
1/2	29.18	0.63	9.99	0.13
1/4	29.18	0.63	9.99	0.12

3.3 Element Comparison

In order to compare the efficiency of the elements, the wall time for each spatial run was gathered and tabulated. The wall time, in seconds, for all of the 8 noded hexahedral formulations is listed in Table 3.19. The order of formulations from fastest to slowest are as follows: mean quadrature, fully integrated, selective deviatoric and Q1P0. The results for the tetrahedral elements is shown in Table 3.20. The efficiency order for these elements is the following: tet4 mean quadrature, tet10 mean quadrature, tet4 nodal based and tet10 fully integrated (tied), and tet10 composite.

Since the number of time steps used in each simulation differs between elements, a better evaluation of element efficiency may be to determine the run time per element per step. This would also provide a way to estimate the run time for a given simulation based on the

Table 3.19. Nonlinear material model, solution wall time (seconds) for hex8 elements with spatial discretization.

	Hex8			
N	Mean Quadrature	Selective Deviatoric	Q1P0	Fully Integrated
2	0.15	0.16	0.19	0.13
4	0.46	0.94	1.36	0.82
8	3.40	12.45	20.22	11.15
16	49.67	198.78	319.54	177.15

Table 3.20. Nonlinear material model, solution wall time (seconds) for tetrahedral elements with spatial discretization.

	Tet4		Tet10		
N	Mean Quadrature	Nodal Based	Mean Quadrature	Fully Integrated	Composite
2	0.65	1.35	1.16	1.45	4.07
4	3.65	12.25	9.23	13.48	263.5
8	61.99	267.38	210.95	280.81	824.18
16	922.06	4577.98	3530.29	4512.20	27771.10

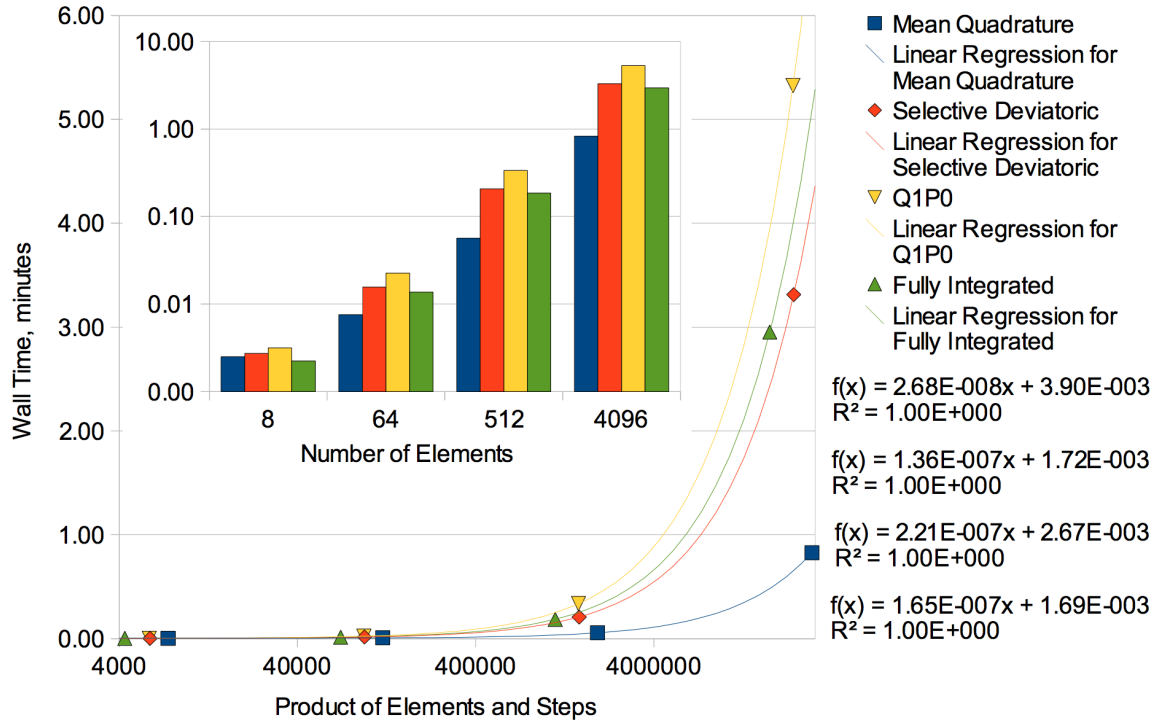


Figure 3.11. Nonlinear material model, hex8 element comparison of wall time.

number of elements and the number of time steps. These values were calculated and plotted against the wall time in minutes. A linear trend line was fitted to the data, and there is a very good match. The results for the hexahedral meshing is shown in Figure 3.11. Note that the units of simulation time in the plot is in minutes, instead of seconds, and will not match the values in Table 3.19. The x axis of the scatter plot is in logarithmic scale, so the data is linear. Also, the wall time versus number of elements is shown in the bar plot. The Y axis on the bar plot is in logarithmic scale, so the time increases exponentially when compared to the element number.

The same results have been plotted for the tetrahedral mesh results, and this is shown in Figure 3.12. The equations for the trend lines are shown inside each figure. They are ordered in the same sequence as the legend. These formulas can be used to estimate the simulation run time for a nonlinear material model.

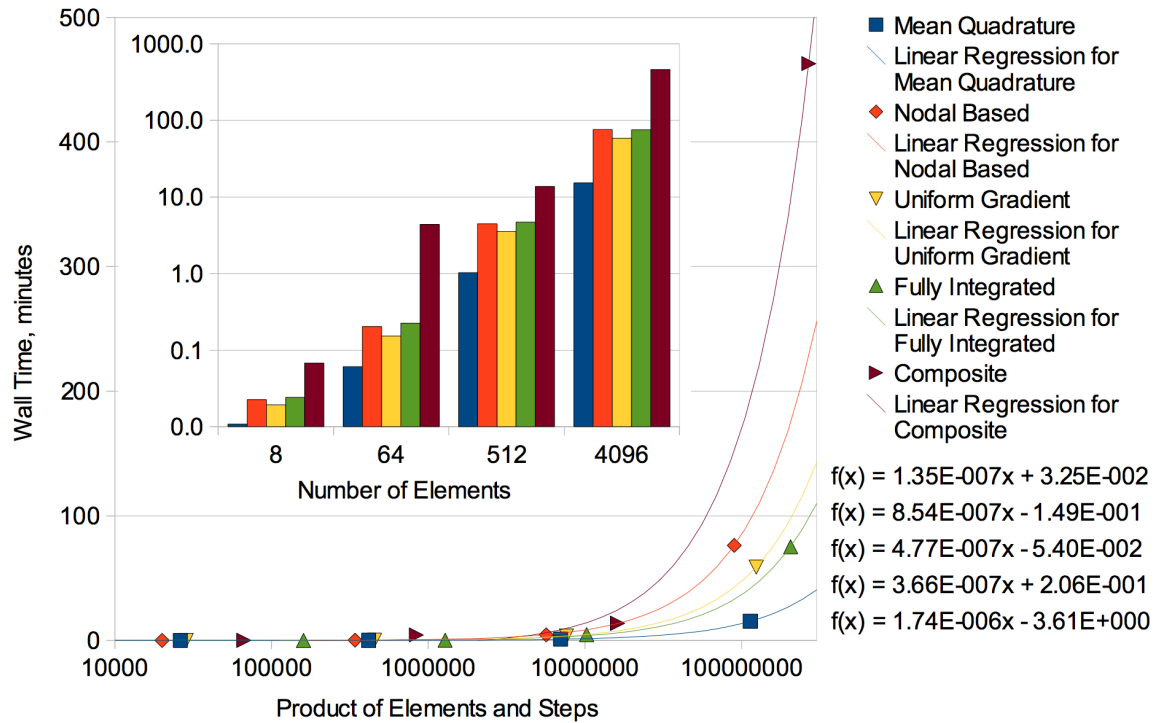


Figure 3.12. Nonlinear material model, tetrahedral element comparison of wall time.

Chapter 4

Impact Model

4.1 Model Description

In this problem, the contact algorithm in explicit transient dynamics is verified for all elements through a simple impact model. A one inch cube and a (5 in x 5 in, x 1 in) plate were created with an offset distance of 0.001 inches in the Z direction. The cube was given an initial velocity of 100 inches per second, while the plate was initially at rest. The termination time was 20 microseconds, and the output variables were saved every microsecond. The solution is verified through the conservation of momentum. Figure 4.1 shows the initial and final displacements of the cube and block. The color scheme corresponds to the displacement from the original position, and the arrows show the direction of the average velocity. The block strikes the plate and is reflected towards the opposite direction, while momentum is transferred to the plate sending it in the positive Z direction.

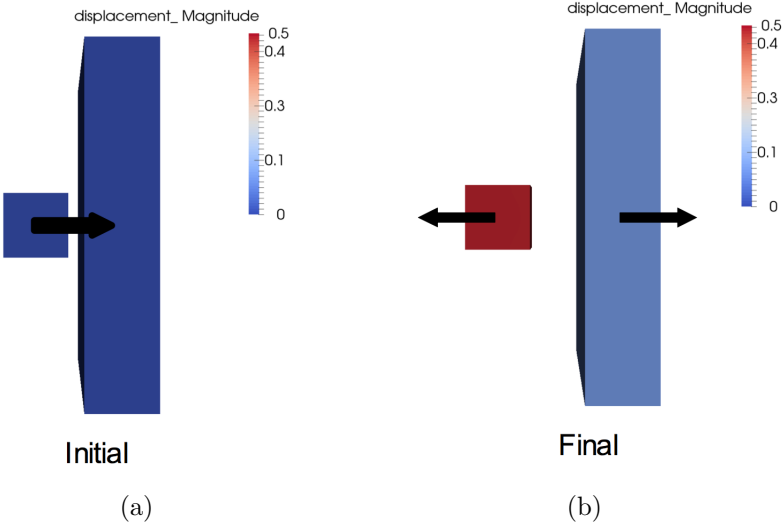


Figure 4.1. Impact model, setup with (a) initial displacements and (b) final displacements.

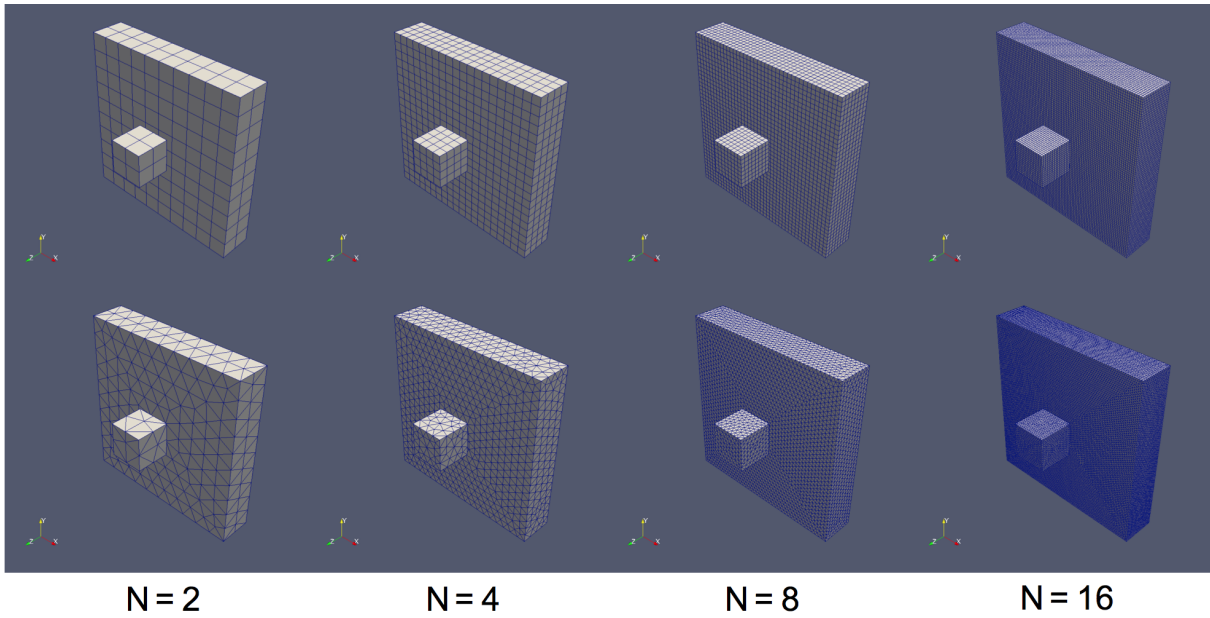


Figure 4.2. Impact model meshing scheme.

The mesh size was controlled by implementing a element size while meshing the components. The element size was controlled by the number of elements through the thickness of the plate and block. The mesh densities used were 2, 4, 8 and 16 elements through the thickness. The meshes are shown in Figure 4.2, where the upper figures are hexahedral meshes and the lower figures are tetrahedral meshes.

The material properties for the hypo-elastic material were as follows: density of $7.4e-4$ sl-inches per cubic inch, Young's modulus of 29 Msi, Poisson's ratio of 0.0. In order to verify the solution, the momentum was compared for each time step to ensure that it remained constant following contact. All of the element cases maintained the same momentum.

4.2 Results

The run times have been plotted for comparison. The results for the hexahedral element are shown in Figure 4.3. The scatter plot shows the product of the number of time steps and the number of elements on the X axis and the wall time in minutes on the Y axis. The X axis is in log scale. A linear trend line has been plotted for each formulation and the equation is shown underneath the legend. There is a good match for each formulation. These equations could be used to estimate run times with impact. The figure also displays a bar graph, where the X axis is the number of elements and the Y axis is the wall time in minutes; the Y axis is in log scale.

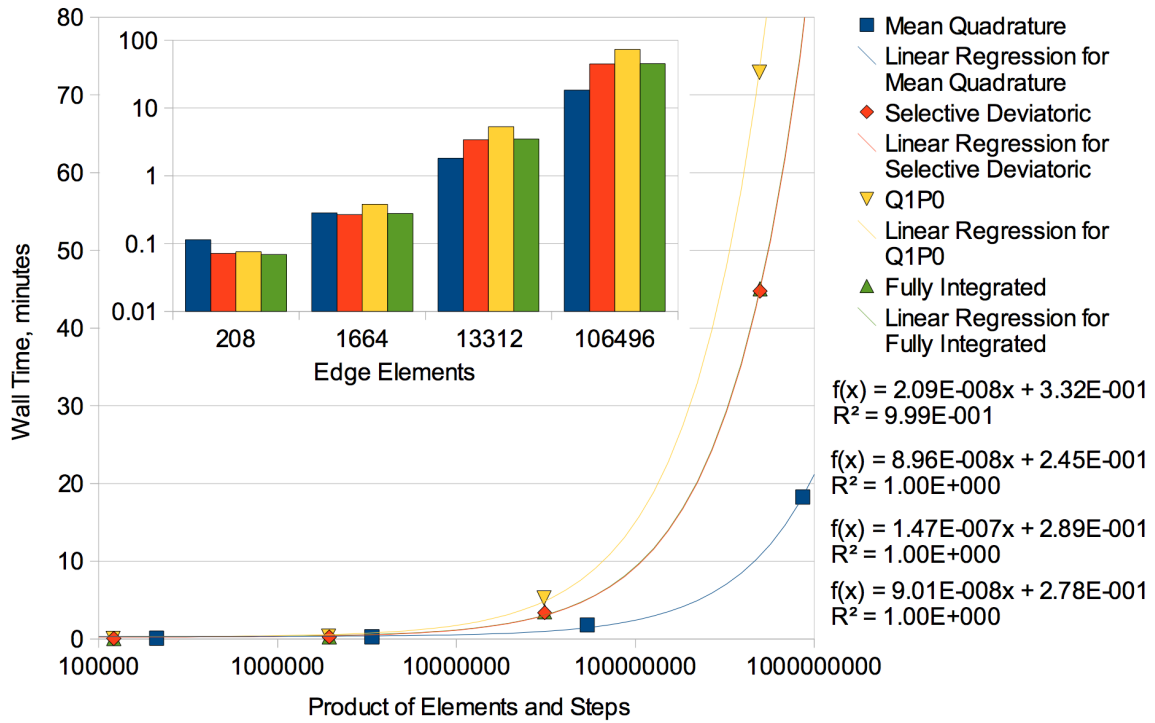


Figure 4.3. Impact model, hexahedral element comparison of wall time.

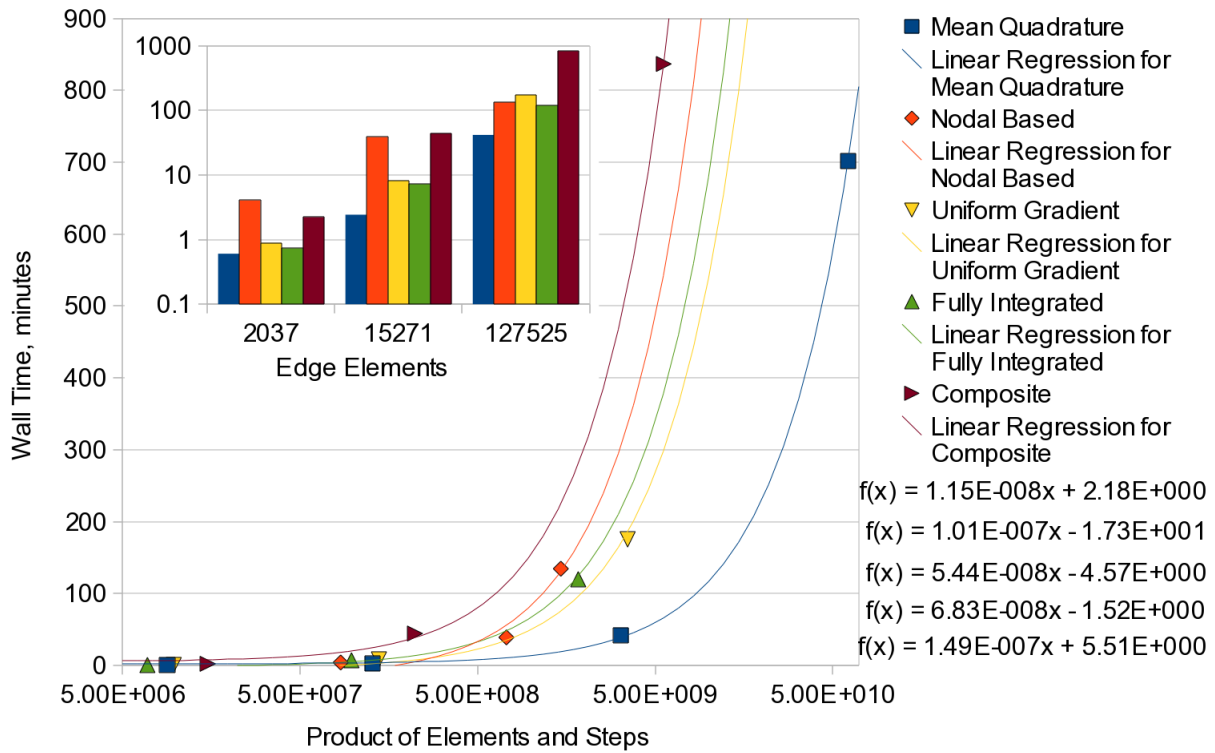


Figure 4.4. Impact model, tetrahedral element comparison of wall time.

The tetrahedral element comparison for the impact model is shown in Figure 4.4. It is clear from the plots that the four noded mean quadrature tet element has a much shorter run time when compared with the other tetrahedral elements. The composite ten noded tetrahedral and nodal based tet are the slowest element formulations, depending on the mesh density, while the remaining two tet10 formulations are closely grouped between the extremes.

Chapter 5

Friction Model

5.1 Model Description

This problem set was performed to verify the use of frictional contact with each element. The model employs gravity to slide a free plate down a second fixed incline plate. The distance traveled at the end of the simulation was compared to the analytical result in order to verify each element. A schematic of the model is shown in Figure 5.1. On the left is the initial displacement, and the right side shows the final displacement. The angle and magnitude of gravity were chosen such that the final displacement should be 0.125 inches. Three mesh refinements were utilized for each type of element. The element size was controlled by varying the number of elements through the thickness of the plates. The sizes used were 1, 2 and 4 elements through the thickness. The mesh refinements are shown in Figure 5.2. This model was run using explicit transient dynamics.

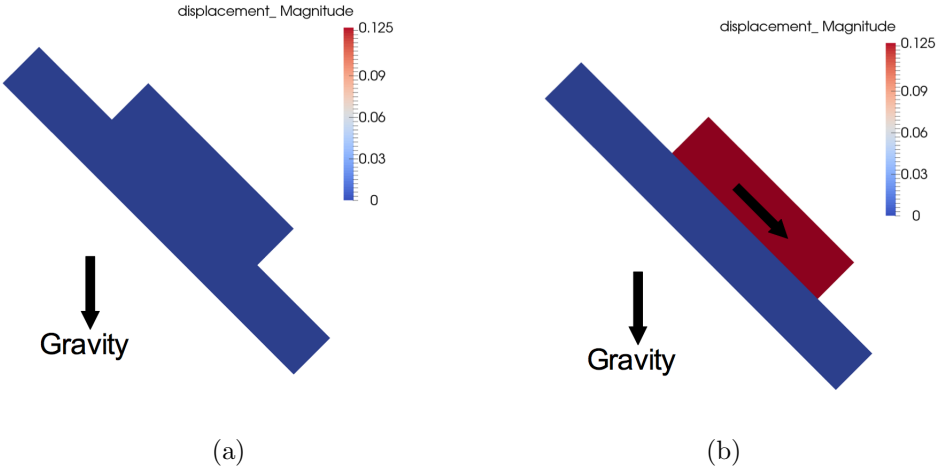


Figure 5.1. Friction model, setup with (a) initial displacements and (b) final displacements.

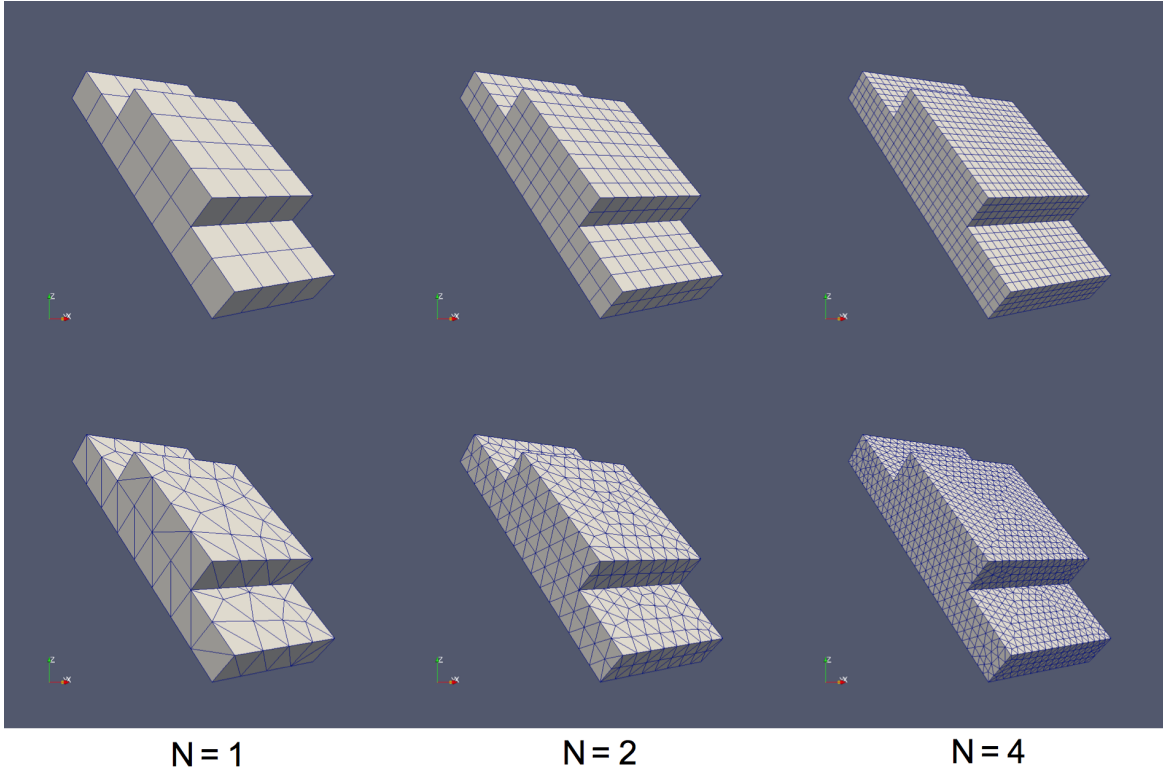


Figure 5.2. Friction model meshing scheme.

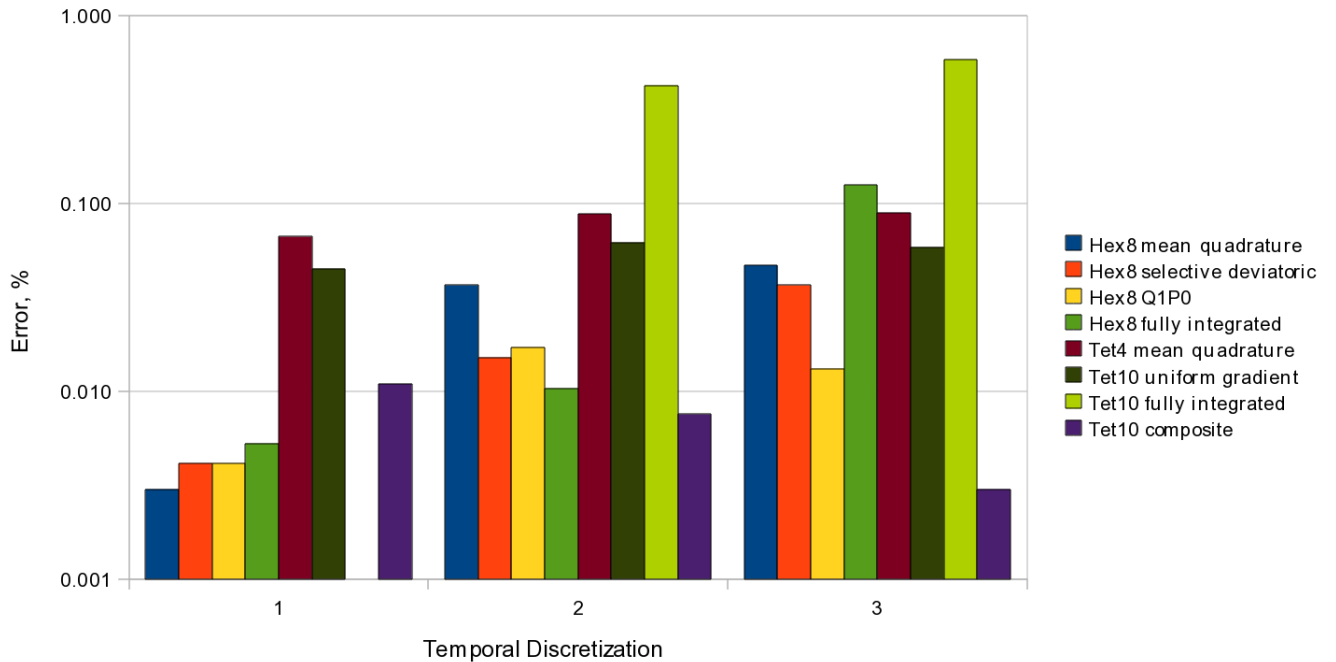


Figure 5.3. Friction model, element comparison of numerical error. The first temporal discretization of the fully integrated tet10 model did not complete; thus, results are not shown.

5.2 Results

The final displacement of the free plate was measured for each problem case and compared to the analytical solution of 0.125 inches. The percent error in the numerical solution for each run is shown in Figure 5.3. All of the results fall below one percent error. Interestingly, increasing the mesh density does not decrease the numerical error. This could be due to the fact that the analytical solution assumes that the plate is a rigid body; however, elastic waves propagate throughout the plate, which could lead to some discrepancies in the final displacement.

As with previous problem sets, the run time was compared across elements. Figure 5.4 shows the wall time, in minutes, against the product of the number of elements and number of time steps divided by the number of CPUs. There is a linear correlation between these values, where each element has a unique scaling factor. For the eight noded hexahedral elements, the most efficient formulation is the mean quadrature, and the least efficient formulation is the Q1P0. The selective deviatoric and fully integrated formulations have very similar run times in between the previous two. However, when only the number of elements is compared to

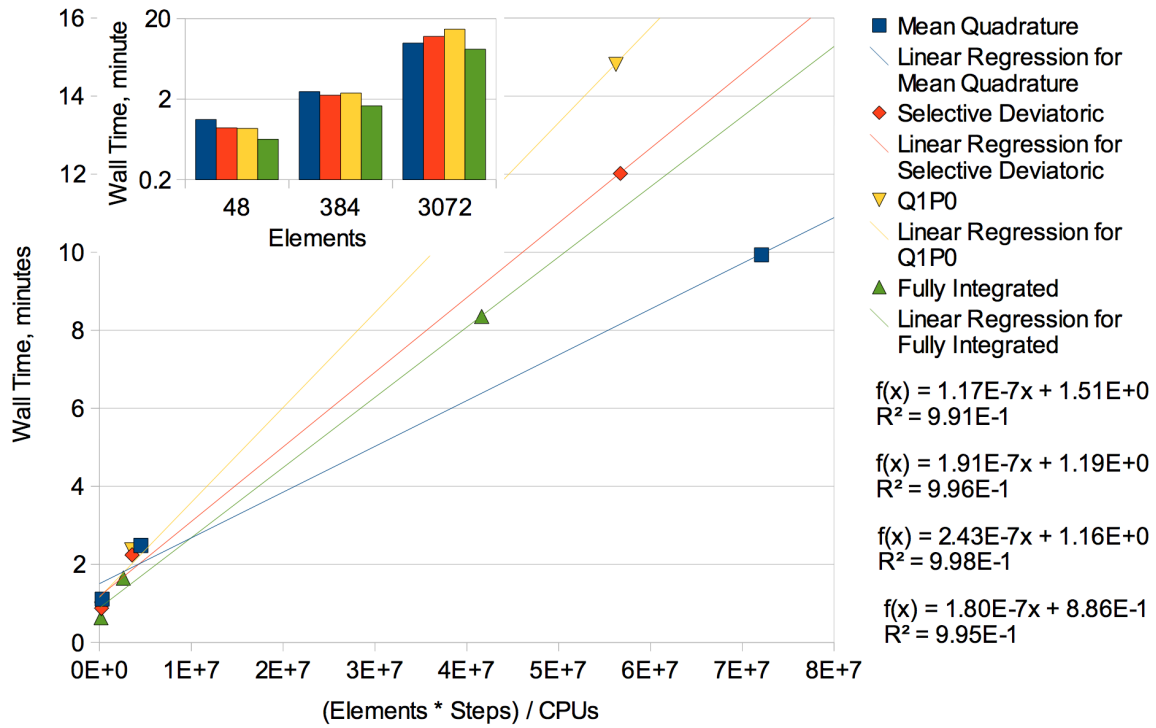


Figure 5.4. Friction model, hexahedral element comparison of wall time.

the wall time, the fully integrated formulation requires the least amount of time to complete the simulation. This again is due to the fact that the fully integrated uses longer time steps, while the mean quadrature uses relatively short time steps. This difference does not appear to affect the results for these simple problems; however, there could be accuracy issues with more complex models.

The same comparison is shown in Figure 5.5 for the tetrahedral elements. The figure shows the results for all of the tetrahedral element formulations. The results indicate that the four noded tetrahedral with a mean quadrature formulation is the most efficient element, while the ten noded composite element is the least efficient. The equation for fitting a linear trend line to the data is shown below the legend. The figure also shows the wall time with respect to the number of elements alone. When only the number of elements is considered, the order of efficiency is rearranged slightly. The fully integrated formulation becomes the second most efficient, while the nodal based and mean quadrature are tied for third, and the composite formulation remains the least efficient. This change in order is due to the fact that number of time steps used for the fully integrated formulation is much less than the others when the automatic time step calculation is requested in the input deck.

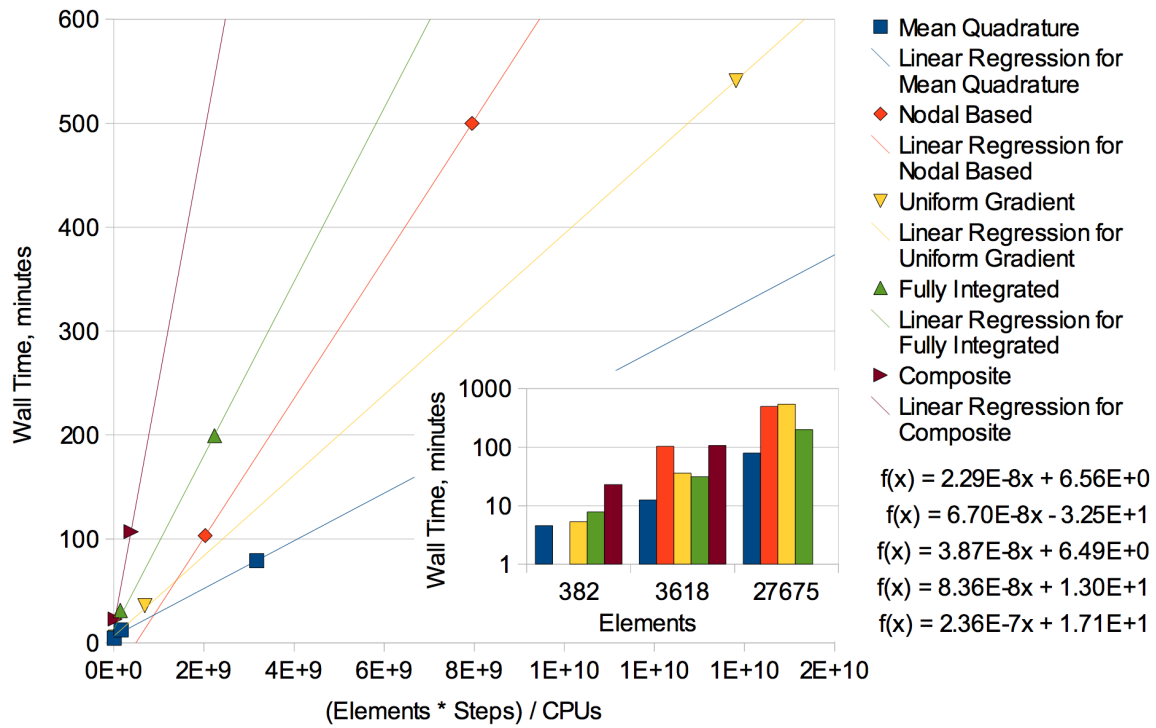


Figure 5.5. Friction model, tetrahedral element comparison of wall time. The 382 element mesh using nodal based tets failed with a segmentation fault, and the composite tet for the most refined mesh did not complete; thus, no results are shown. An updated version of the code may resolve these issues.

Chapter 6

Penetration Model

6.1 Model Description

The penetration model was created to test several capabilities in unison: nonlinear material model, contact and element death. The model utilizes the geometrical symmetry of the problem so that only a quarter of the geometry is modeled. There are two parts in the model, the penetrator, which is one half of a sphere, and a plate. The penetrator is made of copper and is modeled as a linear elastic material. The properties were as follows: the density was 7.764×10^{-9} tonnes per cubic mm, the Young's modulus was 110 GPa and the Poisson's ratio was 0.343. The plate was composed of aluminum and used the BCJ.MEM material model. The material properties and parameters were as follows: density of 2.780×10^{-9} tonnes per cubic mm, Young's modulus of 71.7 GPa, a Poisson's ratio of 0.33, rate dependent yield constant of 350 MPa, isotropic dynamic recovery constant of 9.9, an isotropic hardening constant of 2.69549 GPa, damage exponent of 228, initial damage of 1×10^{-4} , initial void size of 2×10^{-5} , initial void count per volume of 5, and a nucleation parameter 1 of 540. The penetrator was given an initial velocity of three hundred meters per second, and the termination time was one hundred microseconds. The output variables were recorded every microsecond, and the element death criterion was set at damage greater than 0.2. The dimensions for the model are shown in Figure 6.1.

6.2 Results

The penetration model ran using all of the element formulations, performing contact, element death and utilizing the BCJ.MEM material model. The tetrahedral elements were tested using three different mesh refinements. The hexahedral meshes used two different meshing schemes, each with two levels of mesh discretization. The results from each run appear to be unique and different from a run with a different element, spatial discretization or meshing scheme. The most dense meshing schemes begin to show similarities between the tetrahedral element and hexahedral element results. The following sections will show results from each run and the last sections will discuss some comparisons between the elements.

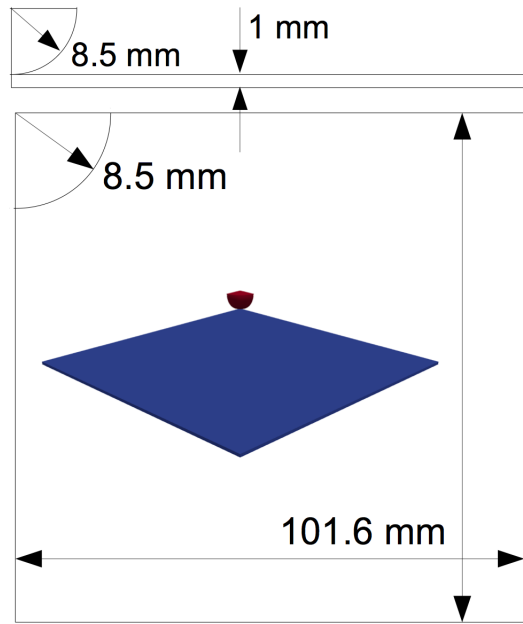


Figure 6.1. Penetration model, setup.

6.2.1 Tetrahedral Discretization 1

The first tetrahedral mesh used a mesh size of 0.5 mm for the penetrator and for the plate underneath the penetrator. The mesh size was then increased up to 2 mm at the far edges of the plate. Since there were only two elements through the thickness of the plate, this mesh has insufficient mesh density and this resulted in artificially large flexural stiffness. Snap shots of the model at the final time step are shown in Figures 6.2 to 6.6. The color scheme shows the magnitude of the von Mises stress. The failure pattern changes between the different formulations, and the stress field appears to be a bit scattered and broken, likely due to the insufficient mesh density.

6.2.2 Tetrahedral Discretization 2

The second mesh discretization decreased the small mesh size to 0.25 mm and the largest mesh size to 1 mm. This increased the number of elements through the thickness to four. The von Mises stress field and deformed geometry are shown in Figures 6.7 to 6.11. These results show a much smoother stress field, and the plastic zone in front of the crack tips are now visible. Also, the crack propagation pattern appears more appropriate. There are still some differences between the results; however, the number of fractures is now uniform at three.

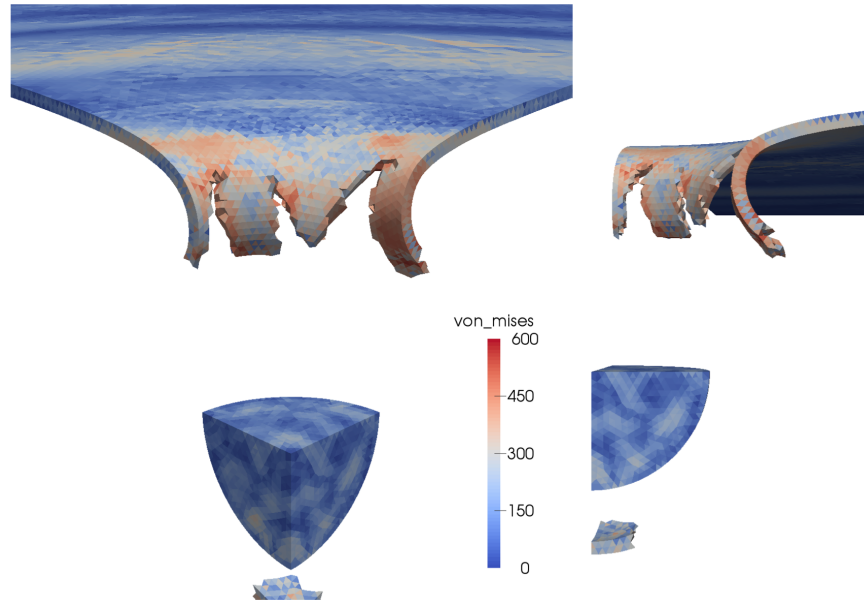


Figure 6.2. Penetration model, tet4 mean quadrature, discretization 1.

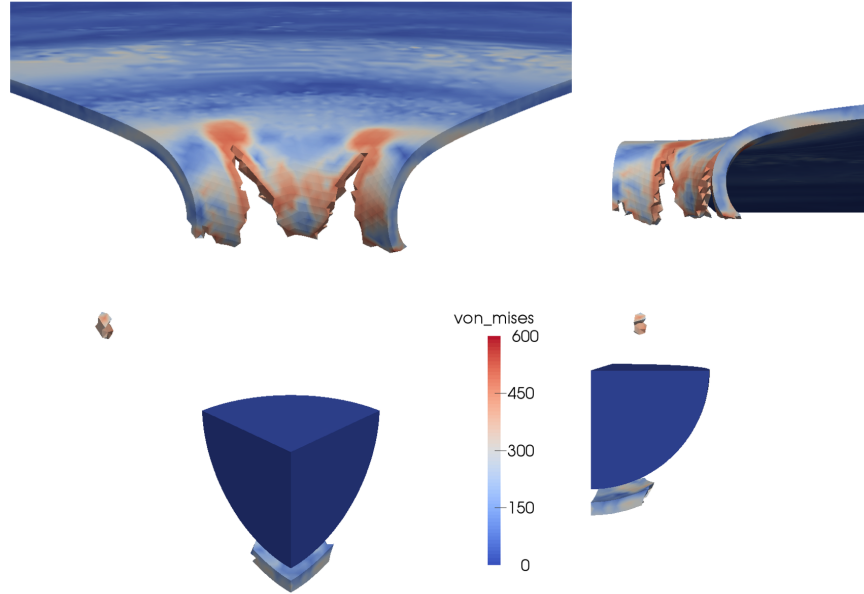


Figure 6.3. Penetration model, tet4 nodal based, discretization 1.

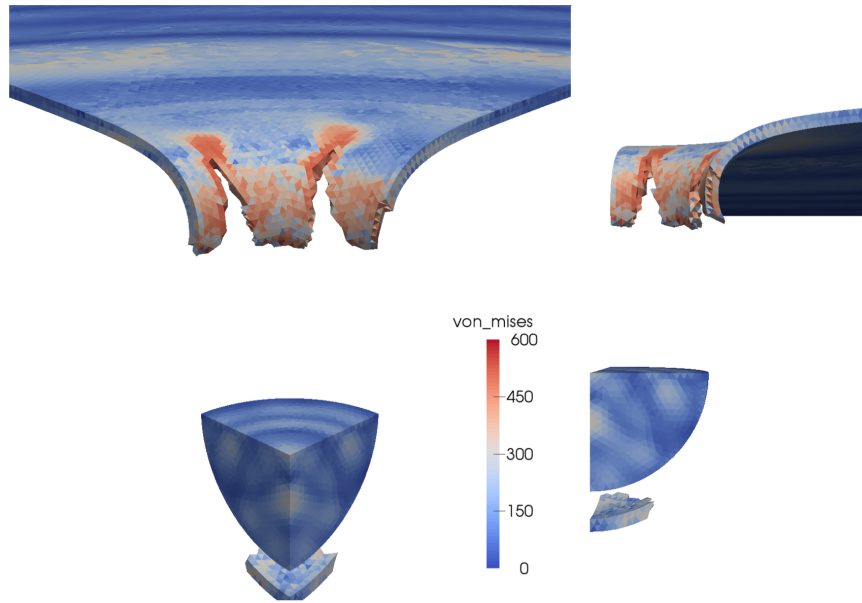


Figure 6.4. Penetration model, tet10 mean quadrature, discretization 1.

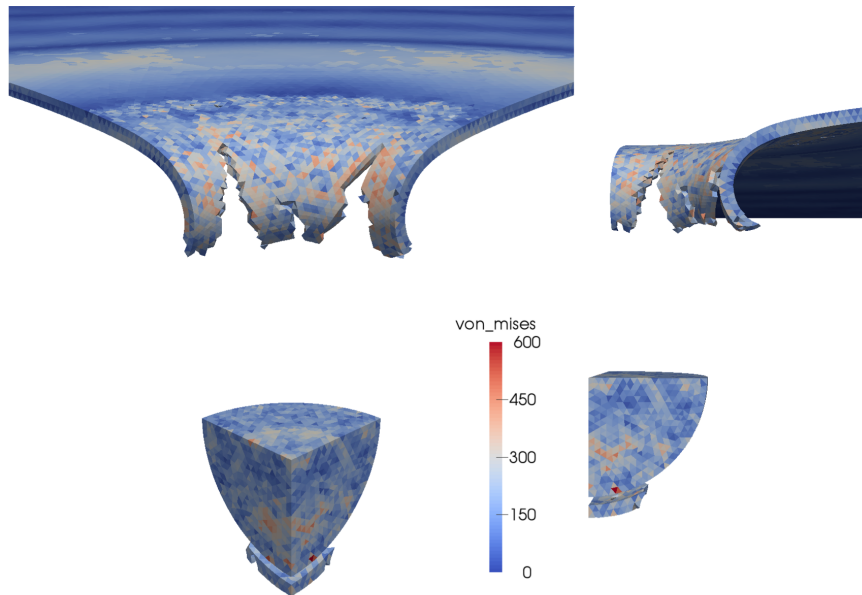


Figure 6.5. Penetration model, tet10 fully integrated, discretization 1.

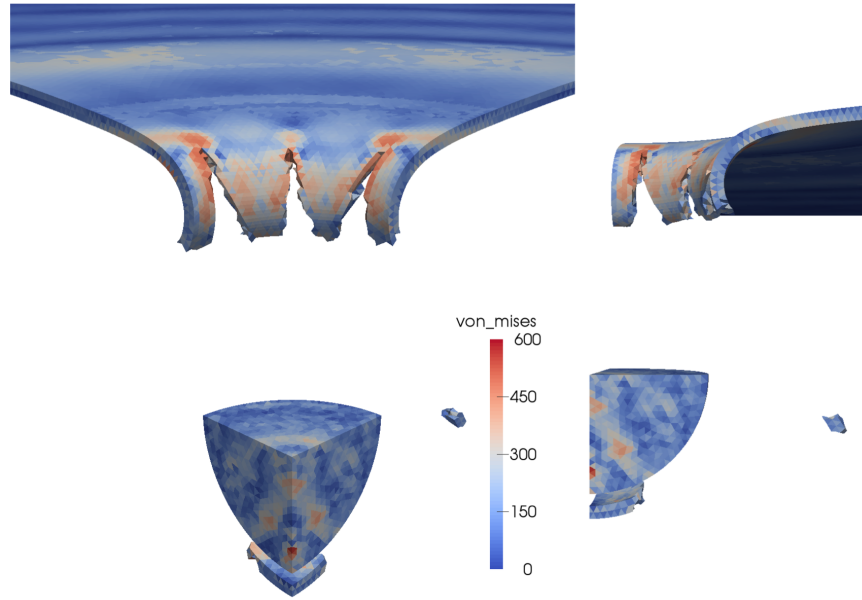


Figure 6.6. Penetration model, tet10 composite, discretization 1.

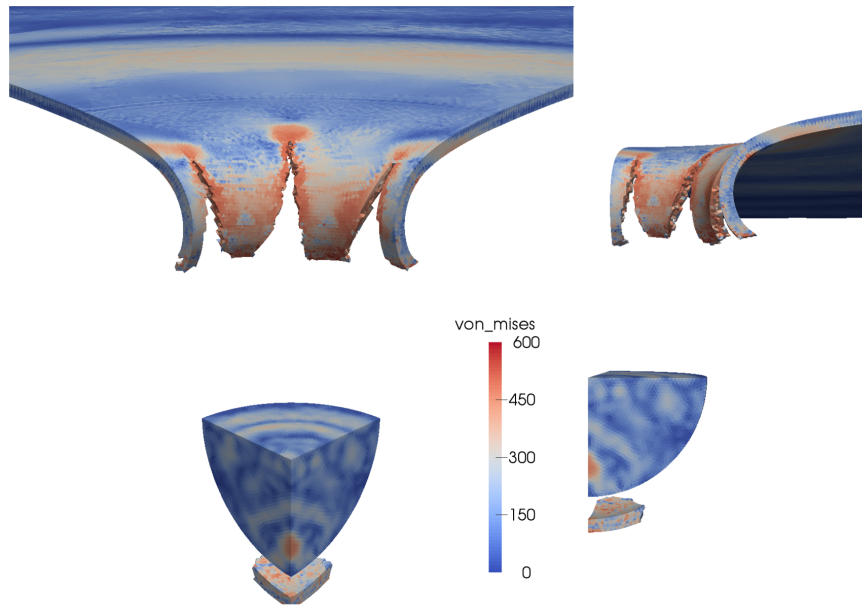


Figure 6.7. Penetration model, tet4 mean quadrature, discretization 2.

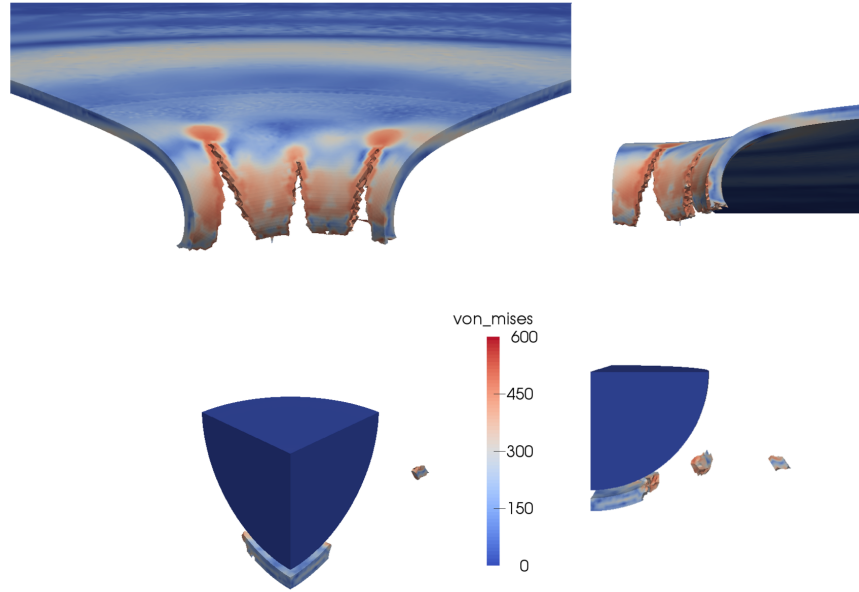


Figure 6.8. Penetration model, tet4 nodal based, discretization 2.

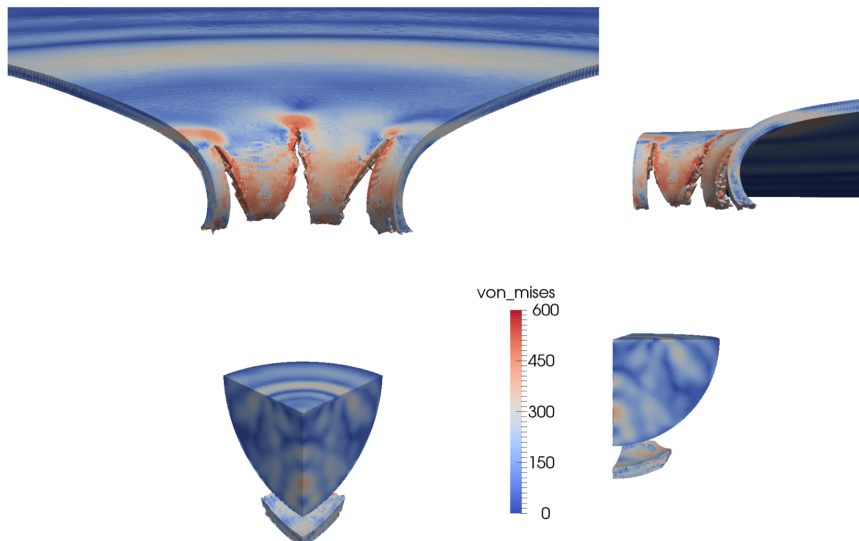


Figure 6.9. Penetration model, tet10, mean quadrature, discretization 2.

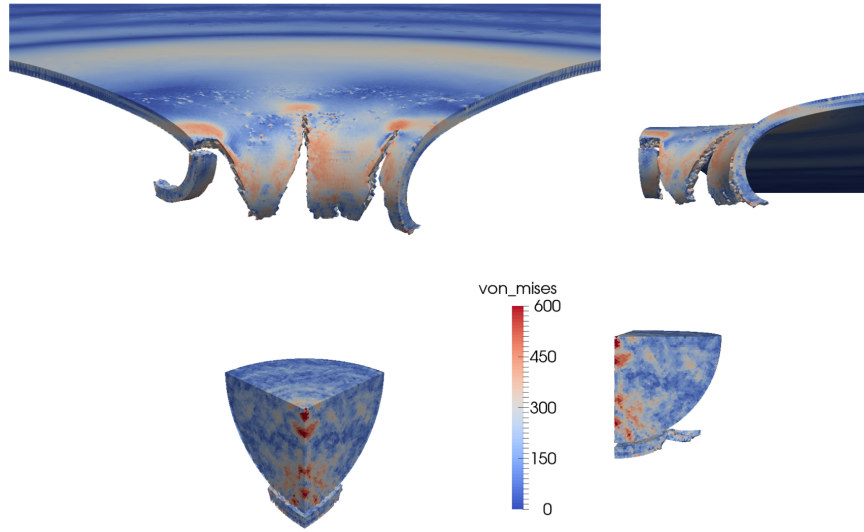


Figure 6.10. Penetration model, tet10, fully integrated, discretization 2.

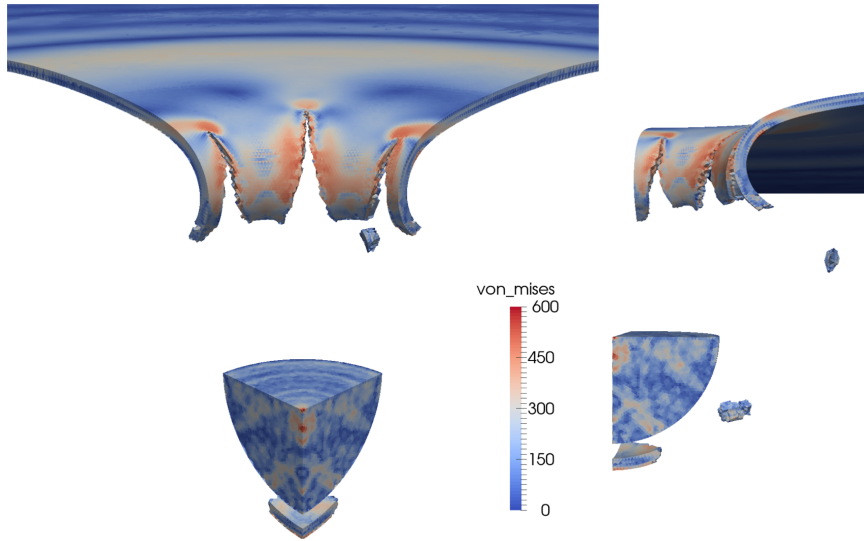


Figure 6.11. Penetration model, tet10, composite, discretization 2.

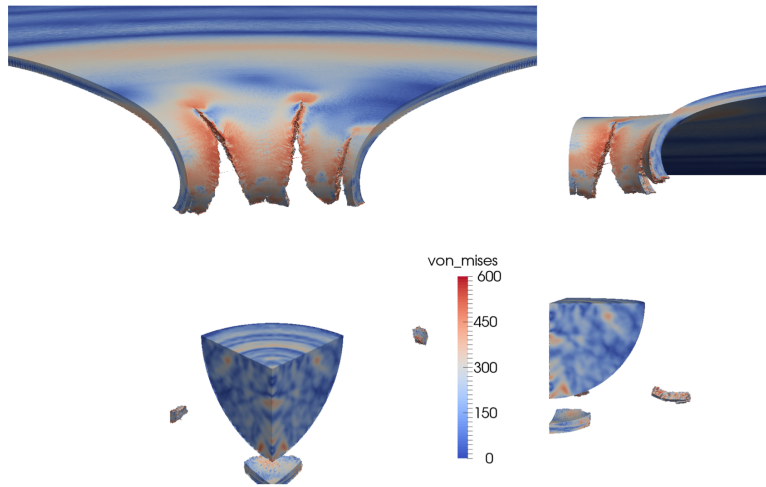


Figure 6.12. Penetration model, tet4, mean quadrature, discretization 3.

6.2.3 Tetrahedral Discretization 3

In the third and final discretization the small mesh size was 0.125 mm and the large mesh size remained at 1.0 mm. The number of elements in this mesh is 3.8 million. As a result, only the two tet4 element meshes completed the simulation in a reasonable amount of time. The remaining three tet10 element models were run with restart files several times, but either never finished or began to produce critical errors. The results for the four noded elements are shown in Figures 6.12 and 6.13. The fracture pattern differs between the two models.

6.2.4 Hexahedral Mesh 1

The first hexahedral element mesh used a small mesh size of 0.5 mm and a large mesh size of 2.0 mm. Also, the number of elements through the plate thickness was set to three. Once again snapshots from the final time steps were collected for all of the element formulations and shown in Figures 6.14 to 6.17. The color scheme corresponds to the magnitude of the von Mises stress. The mean quadrature, Q1P0 and fully integrated formulations have similar fracture patterns, where the crack travels close to the planes of symmetry and propagates radially outward. With the Q1P0 and fully integrated formulations, the petals have begun to break away from the plate. The selective deviatoric formulation has a much different result. In addition to the two fractures, elements have died along the planes of symmetry. Also, the cracks did not propagate as far as the other three formulations.

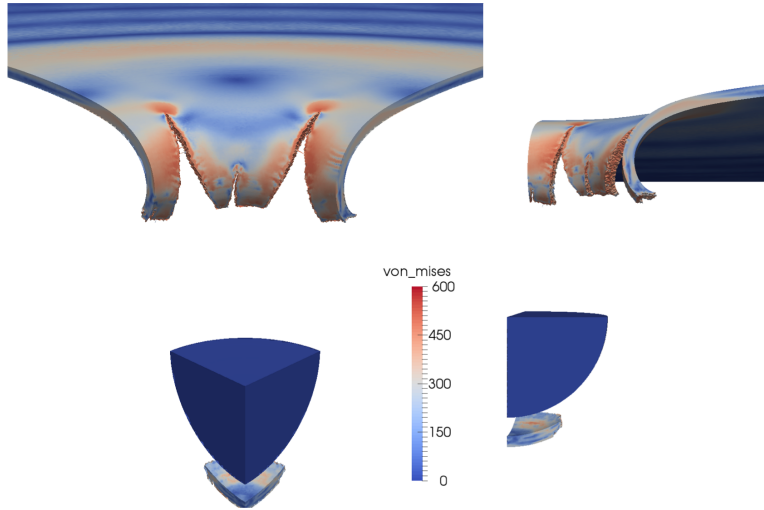


Figure 6.13. Penetration model, tet4, nodal based, discretization 3.

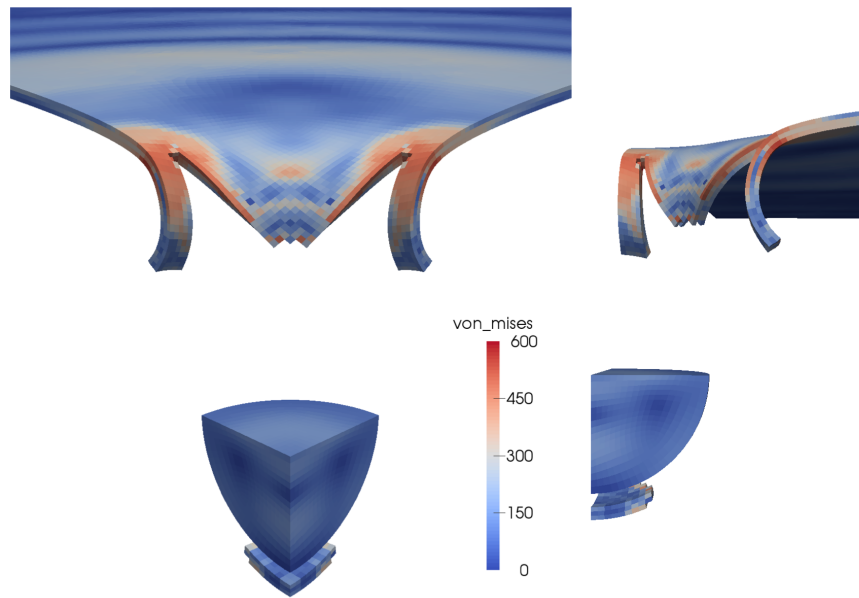


Figure 6.14. Penetration model, hex8, mean quadrature, mesh 1, discretization 1.

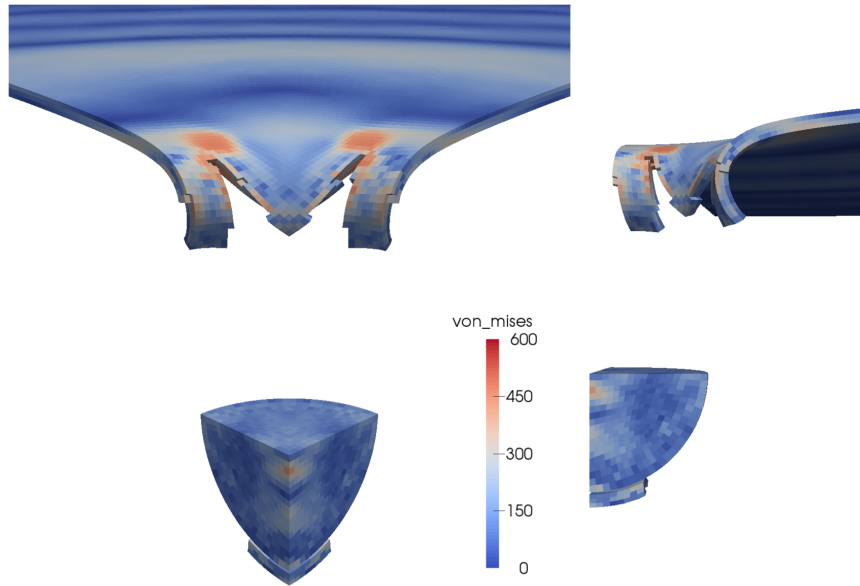


Figure 6.15. Penetration model, hex8, selective deviatoric, mesh 1, discretization 1.

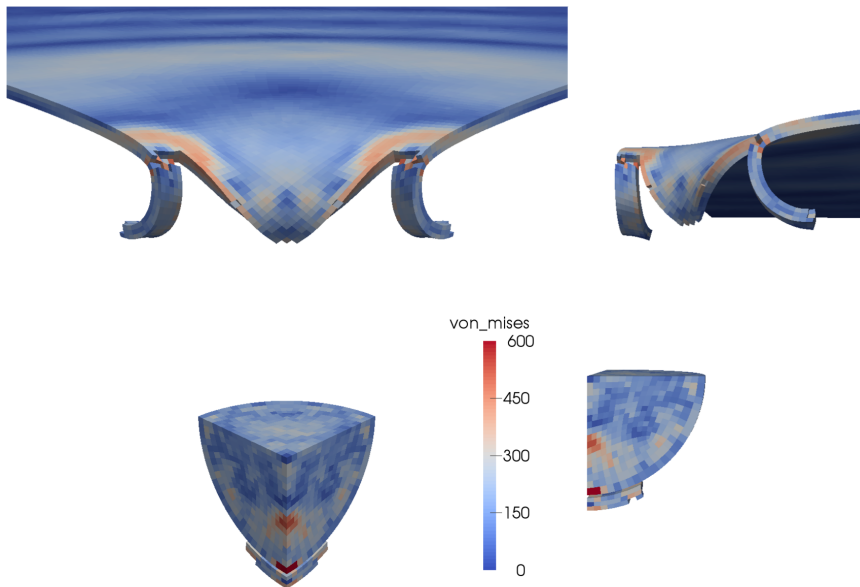


Figure 6.16. Penetration model, hex8, Q1P0, mesh 1, discretization 1.

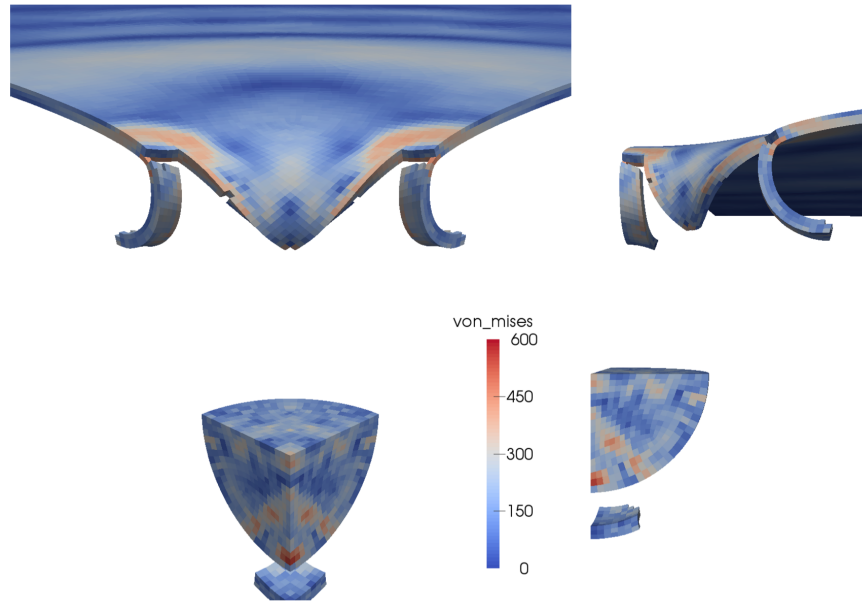


Figure 6.17. Penetration model, hex8, fully integrated, mesh 1, discretization 1.

6.2.5 Mesh Dependence

After the first hexahedral element run, it became clear that the fracture patterns were dependent on the meshing scheme. Therefore, a new meshing scheme was devised in order to provide a better chance for cracks to propagate radially from the center of the plate in a similar manner to the cracks seen with the tetrahedral elements. The new and old meshing schemes are shown in Figure 6.18. The left side of the figure shows the original meshing scheme. This was created in Cubit, where a polyhedral meshing scheme was employed to mesh the portion of the plate nearest to the penetrator. Then, a mapped mesh was used for the remainder. From the plot, it is clear the fracture patterns followed mesh lines. The right side of the figure shows the new meshing scheme. In this scheme, the polyhedral meshing zone was decreased in size, so that it was only the region directly under the penetrator. The mesh size was also decreased to provide more regions to initiate the crack propagation. Then, the mesh was mapped in the remaining plate so that the meshing lines extend radially. This should allow the cracks to propagate radially, as in the tetrahedral models.

In order to further test the original meshing scheme, a refined model was created with a mesh that was twice as dense. Only the mean quadrature formulation was used. The results of this run are shown in Figure 6.19. The left side of the figure shows the results for the first mesh discretization, and the right side of the figure shows the results for the second mesh discretization. The second run does have a third fracture near the middle of the one quarter plate; however, the fracture does not propagate very far. The main fracture points are near

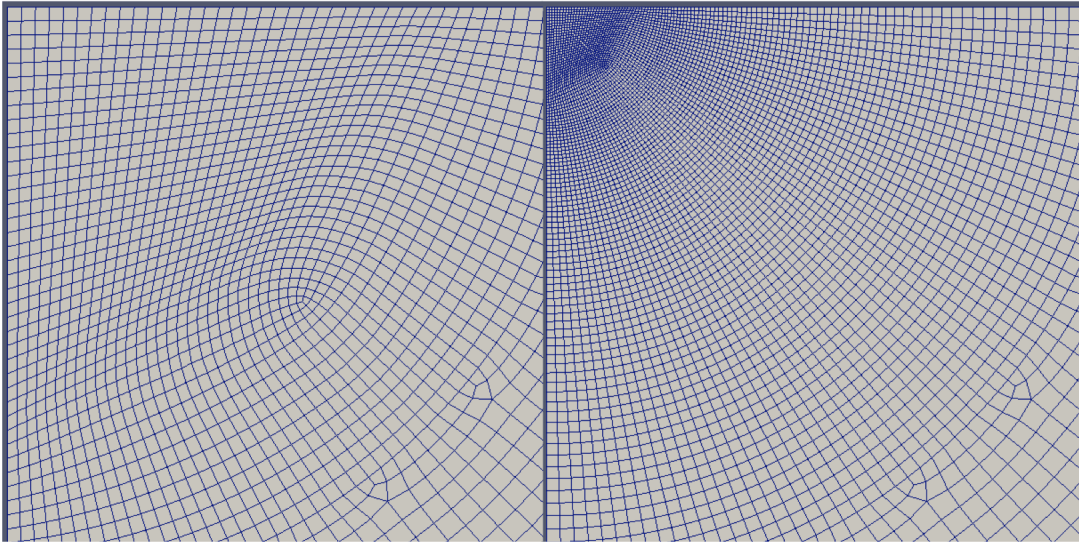


Figure 6.18. Penetration model, comparison of hex meshing schemes, mesh 1: "square" (left) and mesh 2 "radial" (right).

the planes of symmetry, as before, and they propagate even further and begin to break away from the plate.

6.2.6 Hexahedral Mesh 2 Discretization 1

The results of the first discretization of the radial hexahedral mesh are shown in this section. The meshing scheme is the same as described in the previous section with the addition that four elements were used through the thickness of the plate. The results are shown in Figures 6.20 to 6.23. The fracture pattern changes dramatically from the previous results to the current meshing scheme. The number of fractures has increased to about three, and the location and direction of propagation has changed. In addition, it appears that there are waves propagating in the petals, which was not seen in the tetrahedral mesh models.

6.2.7 Hexahedral Mesh 2 Discretization 2

A second mesh discretization was employed for the radial hexahedral meshing scheme. In these models, the mesh sizes have been halved and the number of elements through the thickness has been increased to eight. The results are shown in Figures 6.24 to 6.27. The resulting fracture pattern has become more similar between element formulations with the increased mesh density. However, a phenomenon occurred in the mean quadrature results,

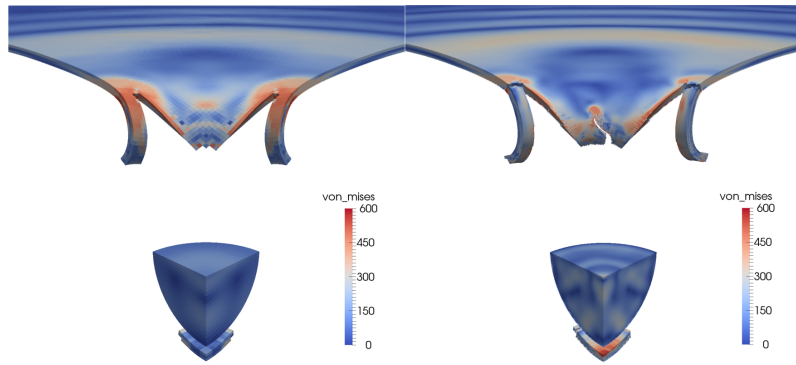


Figure 6.19. Penetration model, mean quadrature hex8 mesh 1, increasing discretization (left to right).

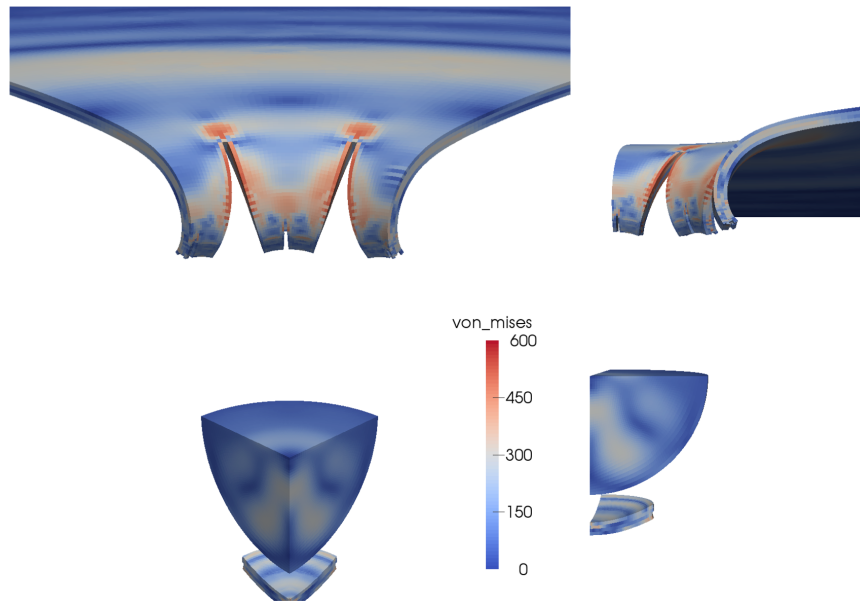


Figure 6.20. Penetration model, mean quadrature hex8 mesh 2, discretization 1.

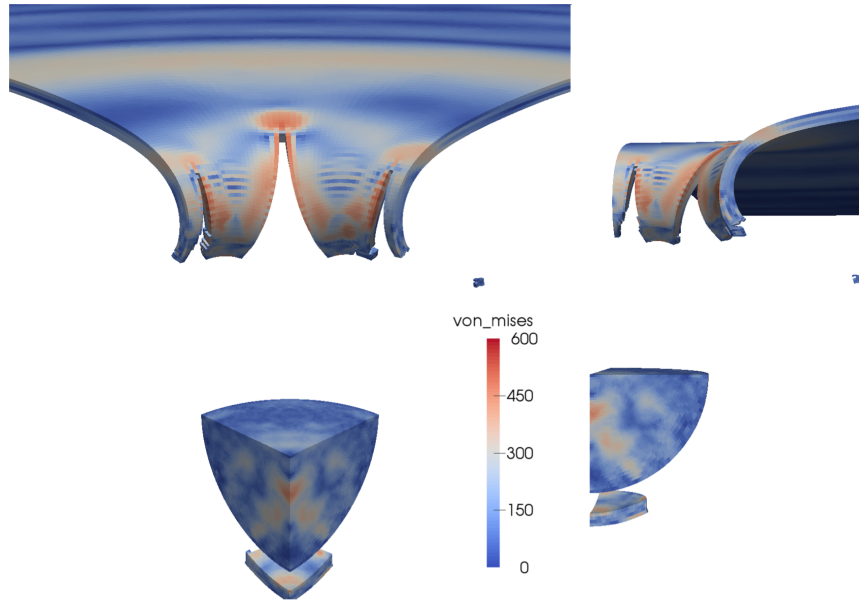


Figure 6.21. Penetration model, selective deviatoric hex8 mesh 2, discretization 1.

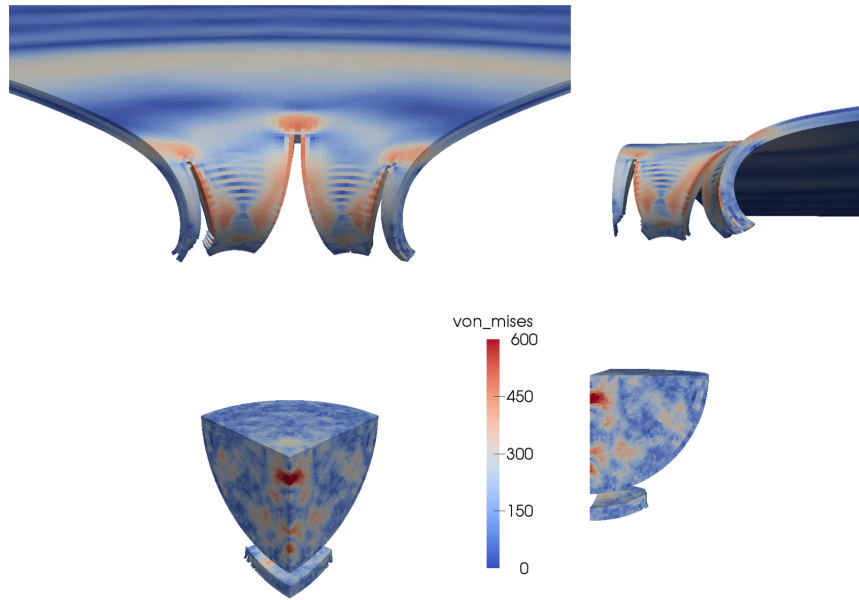


Figure 6.22. Penetration model, Q1P0 hex8 mesh 2, discretization 1.

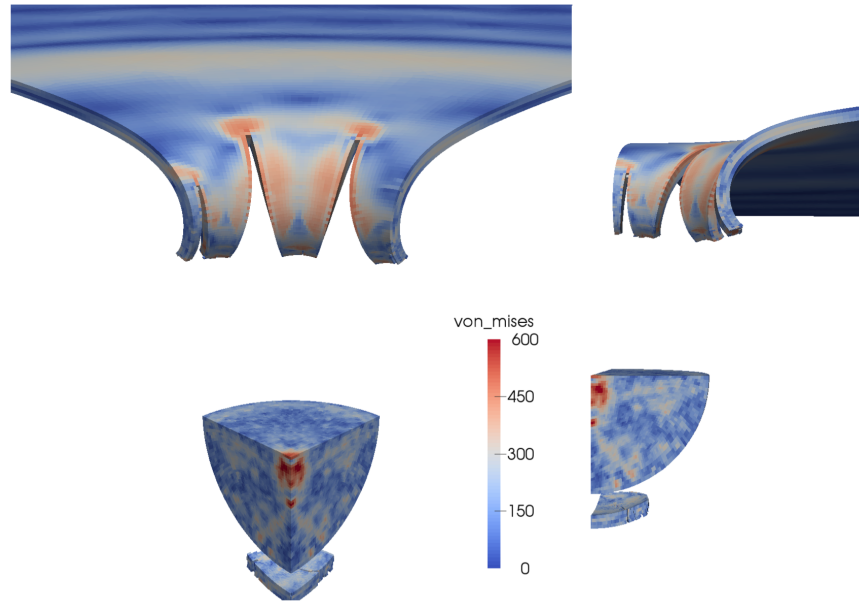


Figure 6.23. Penetration model, fully integrated hex8 mesh 2, discretization 1.

where one of the petals has broken away from the plate. In addition, the fully integrated formulation has multiple pieces of shrapnel which have separated from the plate in addition to the single slug. Another change is that the waves on the petals appear to have a shorter wave length than in the previous results. It is possible that the coarser mesh of the previous scheme did not capture the accurate wavelength.

6.3 Element Comparison

In order to better gauge how the results are altered with changes in meshing scheme and spatial discretization, three metrics were measured for each run. The first metric is the time at which the main piece of shrapnel separates from the plate. The second metric is the time at which the top surface of the penetrator passes below the bottom surface of the plate, and the final metric is the time at which the penetrator is no longer contacting the plate. The results from each run are shown in Figure 6.28. The times for the separation of the first shrapnel is somewhat random without any clear trends; therefore, this must be dependent on both the mesh and the element formulation. The times for the second metric do not vary much, which shows that the velocity after contact does not change much between runs. The velocity by the end of the simulation is around 280 meters per second, which is a small change, so that is why there is such small variation between runs. There is a large change between runs for the time to full penetration, or the third metric. The time decreases as the

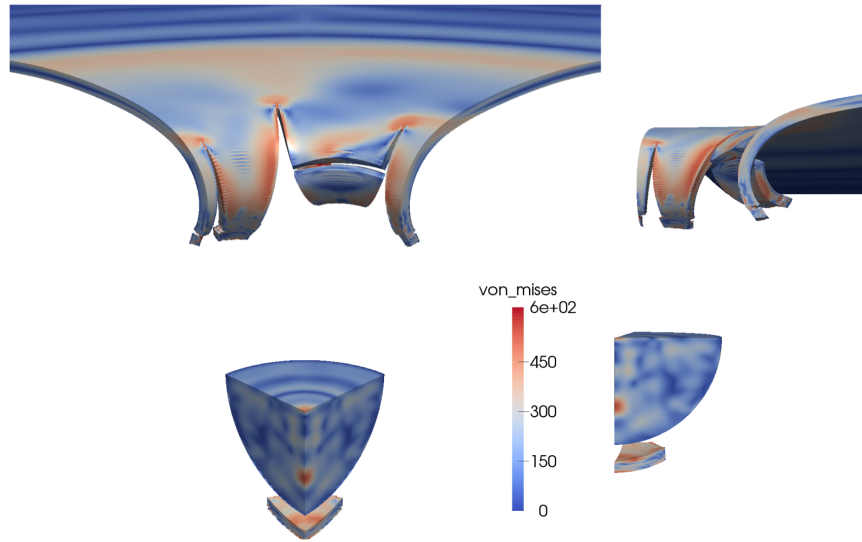


Figure 6.24. Penetration model, mean quadrature hex8 mesh 2, discretization 2.

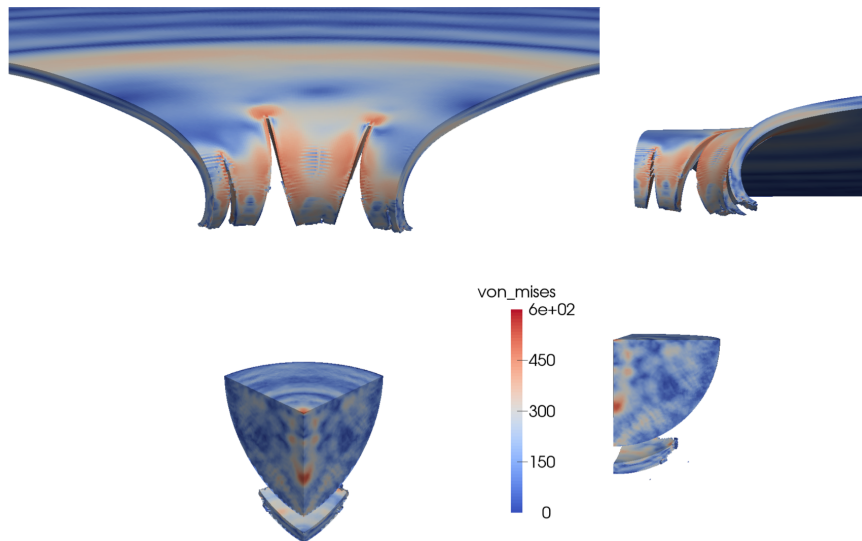


Figure 6.25. Penetration model, selective deviatoric hex8 mesh 2, discretization 2.

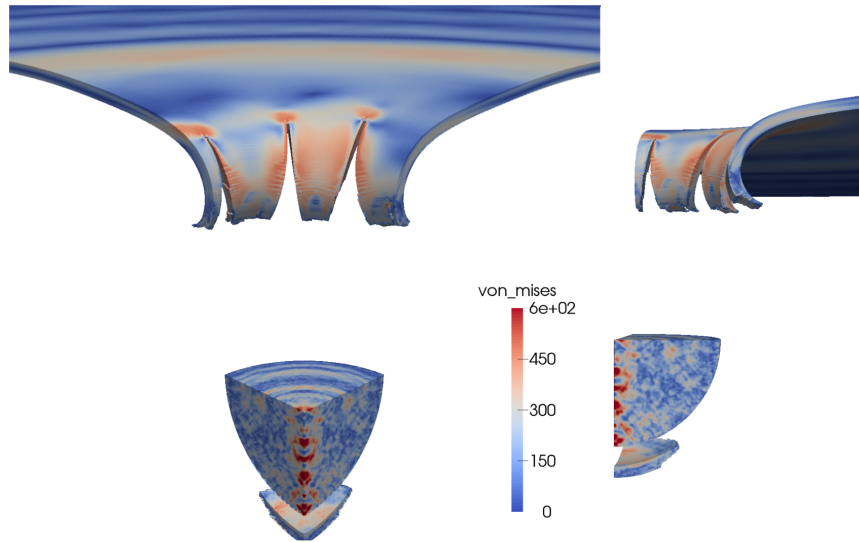


Figure 6.26. Penetration model, Q1P0 hex8 mesh 2, discretization 2.

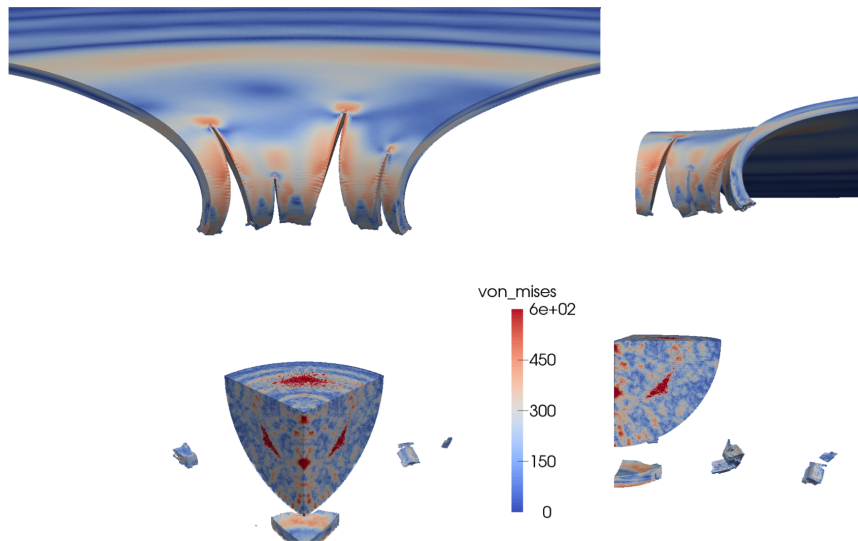


Figure 6.27. Penetration model, fully integrated hex8 mesh 2, discretization 2.

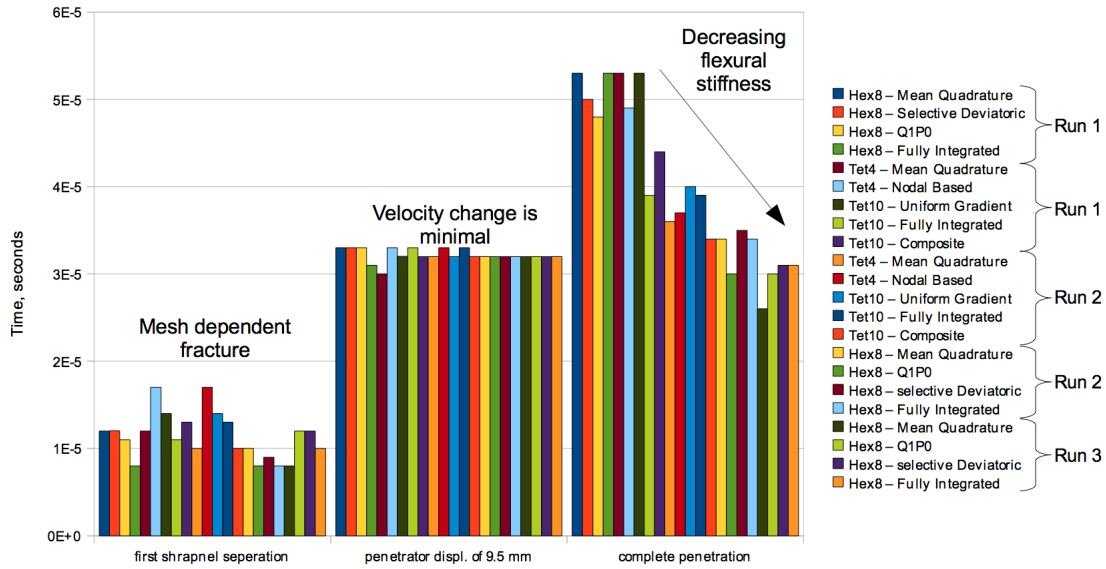


Figure 6.28. Penetration model, comparison between elements.

mesh density increases. This could be due to an artificially large stiffness when there is an insufficient number of elements through the thickness of the plate. As the number of element increases, the flexural stiffness decreases and the penetrator pierces through the plate in less time. In addition, as element death captures fracture energy over the element's volume, the energy needed for fracture decreases with decreasing element size.

In order to evaluate the efficiency of each element formulation, the run time, in hours, has been plotted against the product of the number of elements and the number of time steps divided by the number of CPUs. The results for the hexahedral elements are shown in Figure 6.29, while the tetrahedral results are shown in Figure 6.30. As with the previous simulations, the mean quadrature formulation is the most efficient. For the hexahedral elements, the selective deviatoric formulation is the least efficient, and for the tetrahedral elements the composite formulation is the least efficient.

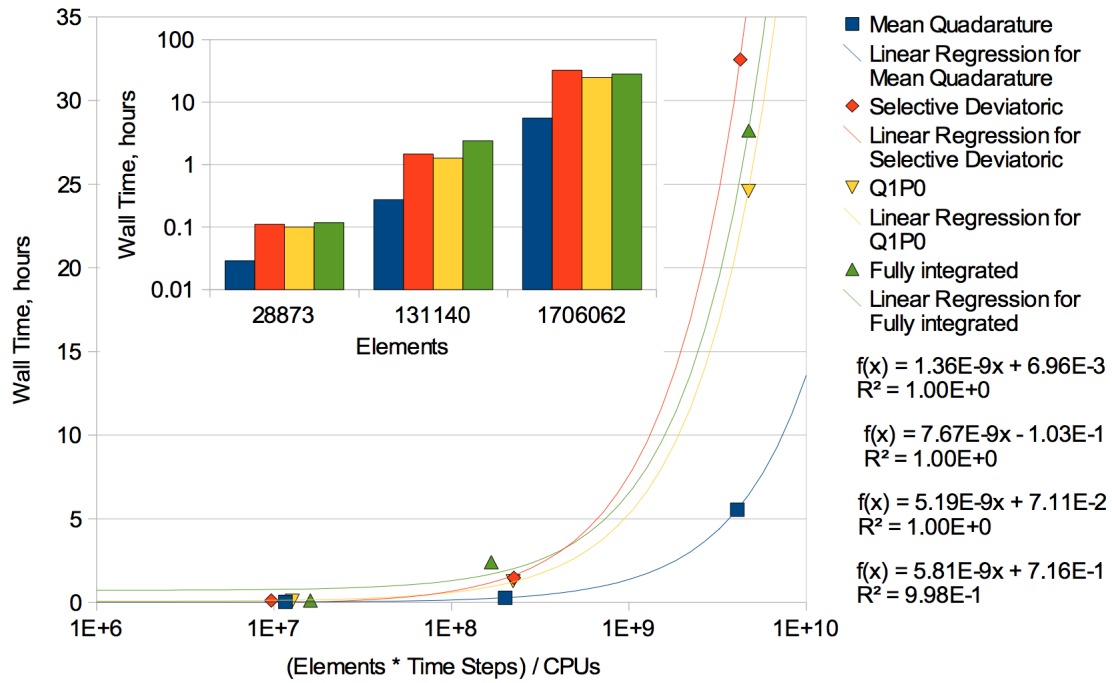


Figure 6.29. Penetration model, hex element comparison of wall time.

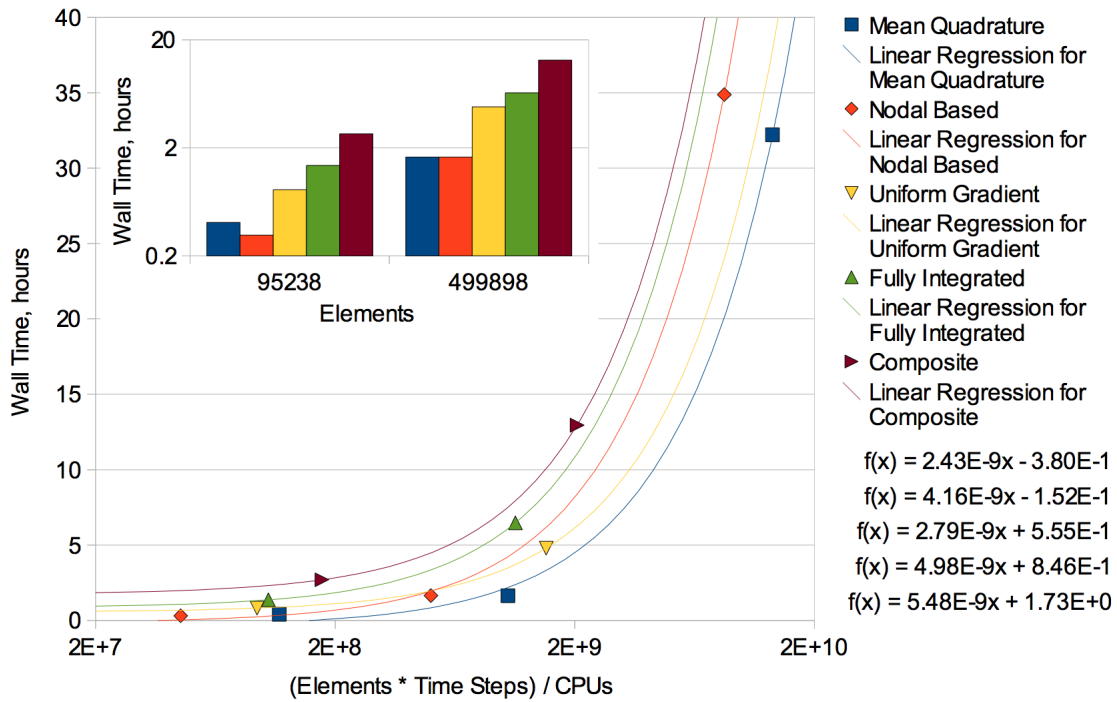


Figure 6.30. Penetration model, tet element comparison of wall time.

Chapter 7

Conclusions

Of the five implicit and explicit problems tested, the behavior of the nine elements used varied; however, some trends emerged. The mean quadrature hex8 element is unsurprisingly the fastest of the 4 hexahedral elements tested, often by far. However, for the friction case, the mean quadrature element was the slowest for the lower mesh density runs and second to the fully integrated hex8 for the most refined mesh. The difference in timing between the elements was not significant, so the results could easily be affected by other factors. The Q1P0 was typically the slowest of the four hex element formulations used, except for the large scale penetration model, in which case it performed similarly to the fully integrated and the selective deviatoric elements. The selective deviatoric and fully integrated elements typically were similar in run times and fell in between the slowest and fastest hex element formulations. In all of our test problems, a deviatoric parameter of 0.5 was used for the selective deviatoric element formulation.

The tetrahedral elements had some more variations between runs, but overall, the standard tet4 elements yielded the lowest compute times. The standard tet10 element and the fully integrated tet10 usually were similar in run times and fell in the middle of the timing studies. The nodal based tets and the composite tets were usually the slowest, often by a significant amount, with some exceptions. Both the nodal based tet and the composite tet required some time step and convergence criteria adjustments in order to run, so the longer run times may be due to that. For the penetration studies, the nodal based tet was the fastest. It is unclear why this is the case. The composite tet also has an outstanding instability, as of Sierra v4.38.1, that resulted in needing a particular number of processors to run; it has been theorized that the fix may also affect the convergence and thus the run times.

Analysis speed is not the only factor when choosing an element; element performance is also of utmost importance. While the errors calculated in the first four studies may be small across the board, the actual metrics of interest for a given problem may not perform as well across all element types. For example, some elements may not adequately capture the stress state while others may be more prone to locking under certain loading conditions; these behaviors may not have been fully captured in this study.

References

- [1] SIERRA Solid Mechanics Team. *Sierra/SolidMechanics 4.36 User's Guide*, Sandia National Laboratories Report 2015-2199, March, 2015.

DISTRIBUTION:

1	MS 0346	R.D.Teeter, 1556
1	MS 9012	C.Alleman, 8343
1	MS 9042	L.L.Beghini, 8259
1	MS 9042	A.A.Brown, 8259
1	MS 9042	B.C.Collins, 8259
1	MS 9042	J.A.Crowell, 8259
1	MS 9042	G.J.deFrias, 8259
1	MS 9042	J.J.Dike, 8259
1	MS 9042	J.W.Foulk, 8343
1	MS 9042	M.D.Jew, 8259
1	MS 9042	K.N.Karlson, 8259
1	MS 9042	K.L.Manktelow, 8259
1	MS 9042	A.Mota, 8343
1	MS 9042	S.M.Nelson, 8259
1	MS 9042	J.T.Ostien, 8343
1	MS 9042	S.T.Peterson, 8343
1	MS 9042	N.Spencer, 8259
1	MS 9042	M.G.Veilleux, 8259
1	MS 9042	T.J.Vogler, 8343
1	MS 9042	M.Yip, 8259
1	MS 9912	A.A.Hanson, 8259
1	MS 9912	M.Stender, 8259
1	MS 9957	R.E.Jones, 8343
1	MS 9957	X.Zhou, 8343
1	MS 0899	Technical Library, 8944 (electronic copy)

